

# NEURAL GREEN'S FUNCTION ACCELERATED ITERATIVE METHODS FOR SOLVING INDEFINITE BOUNDARY VALUE PROBLEMS\*

SHENGYAN LI <sup>†</sup>, QI SUN <sup>†</sup>, XUEJUN XU <sup>†</sup>, AND BOWEN ZHENG <sup>‡</sup>

**Abstract.** Neural operators, which learn mappings between the function spaces, have been applied to solve boundary value problems in various ways, including learning mappings from the space of the forcing terms to the space of the solutions with the substantial requirements of data pairs. In this work, we present a data-free neural operator integrated with physics, which learns the Green kernel directly. Our method proceeds in three steps: 1. The governing equations for the Green's function are reformulated into an interface problem, where the delta Dirac function is removed; 2. The interface problem is embedded in a lifted space of higher-dimension to handle the jump in the derivative, but still solved on a two-dimensional surface without additional sampling cost; 3. Deep neural networks are employed to address the curse of dimensionality caused by this lifting operation. The approximate Green's function obtained through our approach is then used to construct preconditioners for the linear systems allowed by its mathematical properties. Furthermore, the spectral bias of it revealed through both theoretical analysis and numerical validation contrasts with the smoothing effects of traditional iterative solvers, which motivates us to propose a hybrid iterative method that combines these two solvers. Numerical experiments demonstrate the effectiveness of our approximate Green's function in accelerating iterative methods, proving fast convergence for solving indefinite problems even involving discontinuous coefficients.

**1. Introduction.** Neural operators are widely applied in solving boundary value problems for numerical simulations of real world problems, by parametrizing the operator between infinite dimensional function spaces through neural networks [24, 32]. Despite the computational cost of the neural operator training, attainment of the solution for a new given parameter in the PDE model only necessitates the forward pass of the neural network [31, 35], which allows development of fast solvers. Furthermore, given the known forms of the PDE, they have potential to accelerate traditional numerical solvers [2, 7], taking advantage of the neural operator as a mesh-free solver.

Current neural operators mainly focus on learning the mapping from data, including DeepONets [35, 27, 36] and the Fourier Neural Operators [31], which have demonstrated effectiveness even in solving unknown PDEs. When prior knowledge of the underlying PDE is available, physics-informed neural operators [33, 46, 16, 37] are proposed, integrating training data with physical information to achieve superior generalization and reduced data demands [2]. Inspired by this, we propose a data-free neural operator that is purely physics-informed, which learns the Green kernel in the physics space when an explicit form of the PDE is provided.

In this work, we reformulate the equations that the Green's function satisfies in the one-dimensional case into an interface problem [43], where the Dirac delta function as the source term is removed. Then we propose a lift-and-embed learning method to embed this interface problem in a higher-dimensional space, where the jump in the derivative is addressed by introducing auxiliary variables. Similar ideas are presented in kernel-trick employed in Support Vector Machines [5, 42]. Although the

---

\*

**Funding:** Qi Sun is supported in part by the National Natural Science Foundation of China under Grant 12201465.

<sup>†</sup>School of Mathematical Sciences, Tongji University, Shanghai 200092, China (2230930@tongji.edu.cn, qsun\_irl@tongji.edu.cn, xuxj@tongji.edu.cn).

<sup>‡</sup>LSEC, ICMSEC, Academy of Mathematics and Systems Science, Chinese Academy of Sciences, Beijing 100190, China; School of Mathematical Sciences, University of Chinese Academy of Sciences, Beijing 100049, China (zhengbowen@lsec.cc.ac.cn)

lifted problem introduces the curse of dimensionality, this challenge can be managed through deep learning techniques [19] based on the universal approximation theorem [20]. Moreover, this strategy does not increase sampling cost as the problem embedded in the lifted space is still solved on a 2-dimensional surface.

After restricting the feature representation to the original 2-dimensional space, the neural Green's function is obtained and employed to develop fast solvers. However, its direct use as the solution operator struggles to achieve high accuracy, particularly compared with traditional iterative solvers. On the other hand, traditional iterative methods, involving the Jacobi, Gauss-Seidel, conjugate gradient and multi-grid methods, face challenges when solving indefinite systems. The GMRES method [40] converges for indefinite systems but still encounters the issues related to numerical instability and expensive computational cost associated with generating Krylov subspaces [9]. Consequently, we construct preconditioners for the GMRES method through the forward pass of our training model, which approximates the inverse stiffness matrix based on the properties of the Green's function [28]. Recent works have focused on developing preconditioners by neural networks [17, 3, 29]. It is important to emphasize that our approach is applicable to a diverse range of differential operators, rather than being tailored to specific equations.

To gain a deeper understanding of the learning behavior of our training model, we theoretically investigate the training dynamics in the eigenspace of the exact Green's function, and prove the spectral bias demonstrating that our training model recovers the frequency components of the Green kernel from low to high. This finding is in consistence with the spectral bias observed in neural networks, as analyzed in previous studies, utilizing NTK theory or Fourier analysis [38, 47, 48]. For further demonstration, We also provide numerical validation by solving the eigenproblem associated with our neural Green's function. This spectral bias contrasts with the smoothing effect of traditional iterative methods, such as the Jacobi method and the Gauss-Seidel method, which suffer from slow convergence or even divergence for low-frequency components. A hybrid iterative method was proposed in [50], combining the DeepONet with traditional iterative solvers to achieve fast convergence for all frequency components. In this work, we integrate the neural Green's function with the damped Jacobi method for the same goal, demonstrating its effectiveness in solving indefinite systems.

The rest of this paper is organized as follows. In Section 2, we begin by reviewing traditional iterative methods for solving indefinite boundary value problems with coefficients that are continuous or exhibit a jump discontinuities, followed with the potential of the Green's function to speed up these traditional solvers. To overcome the issues of obtaining the Green's function, we embed it in a higher dimensional space and propose the lift-and-embed learning algorithm, accompanied by an illustrative example of a Helmholtz equation. We also provide both theoretical analysis and numerical validation on the spectral bias of our training model in Section 3. With the acquisition of the neural Green's function, we construct preconditioners and hybrid iterative methods in Section 4. Numerical experiments on indefinite problems, one with continuous coefficients and another with a piecewise constant coefficient, are demonstrated in Section 5. Finally, conclusions are reached in Section 6.

## 2. Preliminaries.

**2.1. Model Problem Formulation.** In this work, we consider the following indefinite boundary value problem in a bounded domain  $\Omega \subset \mathbb{R}^d$  with a Lipschitz continuous boundary  $\partial\Omega$ :

$$(2.1) \quad \begin{aligned} -\nabla \cdot (c(x)\nabla u(x)) - k^2(x)u(x) &= f(x), & \text{in } \Omega, \\ u(x) &= 0, & \text{on } \partial\Omega, \end{aligned}$$

where  $f(x)$  is a source term defined in  $L^2(\Omega)$ . The coefficient function  $k(x)$  is assumed to be continuous, while  $c(x)$  belongs to  $L^\infty(\Omega)$  and may exhibit piecewise smooth behavior across the interface.

After discretizing (2.1) using finite element or finite difference methods [28], and the immersed interface methods [30] when  $c(x)$  is discontinuous, we obtain a linear algebraic system

$$(2.2) \quad AU = F,$$

where  $A \in \mathbb{R}^{n \times n}$  indicates the stiffness matrix,  $F \in \mathbb{R}^{n \times 1}$  the load vector,  $U \in \mathbb{R}^{n \times 1}$  the vector of unknowns, and  $n \in \mathbb{N}_+$  the degrees of freedom. It is well-known that the convergence of iterative solvers is strongly dependent on the spectral properties of this linear system [41]. However, when  $k^2(x)$  is sufficiently large, the system becomes indefinite, rendering traditional iterative methods such as the damped Jacobi method ineffective. This challenge is exacerbated when the coefficient function  $c(x)$  exhibits a finite jump at the interface.

**AN ILLUSTRATIVE EXAMPLE.** *For the ease of illustration, we consider the benchmark Helmholtz equation in one dimension, that is,*

$$(2.3) \quad \begin{aligned} -u''(x) - k^2u(x) &= f(x), & \text{in } (0, 1), \\ u(0) = u(1) &= 0. \end{aligned}$$

*Based on the partition of domain  $\Omega = [0, 1]$  using equally spaced grid points  $\{x_i = ih\}_{i=0}^{n+1}$  with meshwidth  $h = (n+1)^{-1}$ , the centred difference approximation [28] to problem (2.3) results in the linear algebraic system (2.2) with the differentiation matrix  $A = \text{tri}[-1, 2 - k^2, -1] \in \mathbb{R}^{n \times n}$  and load vector  $F = h^2[f(x_1), f(x_2), \dots, f(x_n)]^T$ . The eigenvalues of matrix  $A$  are given by  $\lambda_j(A) = 4\sin^2(\frac{j\pi}{2n+2}) - k^2$ ,  $1 \leq j \leq n$ , with corresponding eigenvectors  $\xi_j$ ,  $1 \leq j \leq n$ , where the  $p$ th component  $\xi_{j,p} = \sin(\frac{jp\pi}{n+1})$ ,  $1 \leq j \leq n$ ,  $1 \leq p \leq n$ . For increasing wavenumbers  $k$ , the indefinite nature of matrix  $A$  results in both positive and negative eigenvalues.*

**2.2. Smoothing Effects of Classical Iterative Methods.** Here classical iterative methods for solving (2.2) are introduced in a residual-correction form [28]. Starting from an initial guess  $U^{[0]} \in \mathbb{R}^n$ , the update from  $U^{[m]}$  to  $U^{[m+1]}$  in one iteration consists of three steps:

$$1) R^{[m]} = F - AU^{[m]}, \quad (2.4)$$

$$2) E^{[m]} = BR^{[m]} \text{ with } B \approx A^{-1}; \quad (2.5)$$

$$3) U^{[m+1]} = U^{[m]} + E^{[m]}, \quad (2.6)$$

which is terminated until certain stopping criteria are satisfied. Note that the matrix  $B$  is called *iterator* and assumed to be nonsingular. Based on the matrix splitting  $A = \tilde{D} + \tilde{L} + \tilde{U}$ , where  $\tilde{D}$ ,  $\tilde{L}$ , and  $\tilde{U}$  are the diagonal, strictly lower triangular, and strictly upper triangular parts of  $A$ , respectively. For the damped iterative scheme (also known as weighted iterative scheme), as the iteration proceeds, the approximation error satisfies

$$(2.7) \quad U^{[m+1]} - U^* = ((1 - \omega)I - \omega\tilde{D}^{-1}(\tilde{L} + \tilde{U}))(U^{[m]} - U^*) := G_\omega(U^{[m]} - U^*),$$

where  $U^* \in \mathbb{R}^n$  is the exact solution,  $\omega \in \mathbb{R}_+$  is a user-defined relaxation parameter,  $G_\omega = (1 - \omega)I - \omega\tilde{D}^{-1}(\tilde{L} + \tilde{U})$  is the iterative matrix. In the benchmark equation

(2.3), this iterative matrix simplifies to  $G_\omega = I - \frac{\omega}{2-k^2}A$  with its  $j$ th eigenvalue given by  $\lambda_j(G_\omega^J) = 1 + k^2 - \frac{4\omega}{2-k^2}\sin^2(\frac{j\pi}{2n+2})$ ,  $1 \leq j \leq n$ .

For the Laplace operator *i.e.*,  $k = 0$ , eigenvalues in the upper half of the spectrum, specifically,  $\lambda_j(G_\omega)$  for  $\frac{n}{2} \leq j \leq n$ , can be effectively reduced by suitable choice of  $\omega$ . However, for all  $\omega$  in the range  $0 < \omega < 1$ , the eigenvalues associated with lowest modes remain close to 1, leading to slow convergence for the low-frequency components. The multigrid method based on Jacobi relaxations provides a solution and achieves fast convergence for all the frequency components. However, for the Helmholtz operator with a growing  $k^2 > 0$ , the maximum eigenvalues exceed 1, which causes the divergence of it.

To ensure convergence for the indefinite systems, the GMRES method [40] is often employed. By the Cayley-Hamilton theorem, there exists a polynomial  $p_{n-1}(\cdot)$  that satisfies  $A^{-1} = p_{n-1}(A)$ . The original problem (2.2) is then reformulated as a least squares problem in the Krylov subspace:

$$(2.8) \quad \min_{E^{[m]} \in \mathcal{K}_m} \|R - AE^{[m]}\|,$$

where  $\mathcal{K}_m = \text{span}\{R, AR, \dots, A^{m-1}R\}$ . After  $m$  iterations using Arnoldi's method [1] to find the orthonormal basis  $Q_m = \{q_1, q_2, \dots, q_m\}$  of the Krylov subspace  $\mathcal{K}_m$ , we have  $AQ_m = Q_{m+1}\bar{H}_m$ , where  $Q_{m+1} = [Q_m, q_{m+1}]$  and  $\bar{H}_m \in \mathbb{R}^{(m+1) \times m}$  consists of an upper Hessenberg matrix  $H_m \in \mathbb{R}^{m \times m}$  with an additional row that is all zeros except for the  $h_{m+1,m}$  entry. Thus when  $m \ll n$ , the least squares problem (2.8) is reduced to a small least squares problem

$$(2.9) \quad \min_{E^{[m]} \in \mathcal{K}_m} \|R - AE^{[m]}\| = \min_{Y \in \mathbb{R}^m} \|(Q_{m+1})^T R - \bar{H}_m Y\|.$$

Moreover,  $QR$  factorization of  $\bar{H}_m$  is relatively cheap since  $\bar{H}_m$  is nearly upper triangular. The lemma below ensures the convergence of GMRES even for an indefinite  $A$ .

**LEMMA 2.1** (Convergence of GMRES [40]). *Assume  $A$  is diagonalizable *i.e.*  $A = XDX^{-1}$ , where  $D$  is diagonal and  $X$  is invertible. Let  $A$  have  $\nu$  eigenvalues  $\lambda_1, \lambda_2, \dots, \lambda_\nu$  with nonpositive real parts, while the remaining eigenvalues lie within a circle of radius  $\rho < C$  centered at  $C > 0$ . Denote  $\mathcal{P}_l$  as the space of all polynomials of degree  $\leq l$ . Then the following holds:*

$$(2.10) \quad \epsilon^{(m)} = \min_{\substack{p \in \mathcal{P}_l \\ p(0)=1}} \max_{1 \leq i \leq n} |p(\lambda_i)| \leq \left[\frac{D}{d_0}\right]^\nu \left[\frac{\rho}{C}\right]^{m-\nu},$$

where

$$(2.11) \quad D = \max_{\substack{1 \leq i \leq \nu, \\ \nu+1 \leq j \leq n}} |\lambda_i - \lambda_j|, \text{ and } d_0 = \min_{1 \leq i \leq \nu} |\lambda_j|.$$

Furthermore, the residual norm at the  $m$ th step of GMRES satisfies

$$(2.12) \quad \|R^{[m]}\| \leq \kappa_0(X)\epsilon^{(m)}\|R^{[0]}\|,$$

where  $\kappa_0(X) := \|X\|\|X^{-1}\|$  is the condition number of  $X$ .

However, estimating the convergence and optimality property of the GMRES method remains challenging for indefinite systems. Furthermore, constructing the

orthonormal basis when  $m$  is large incurs high computational cost and memory demands. Even with restart techniques, selecting appropriate restart parameters is difficult [9]. Therefore, introducing suitable preconditioners tailored to specific problems is essential.

**2.3. Deep Learning of Green's Function.** Note that the solution of model problem (2.1) can be analytically obtained through

$$(2.13) \quad u(x) = \int_{\Omega} G(x, y) f(y) dy,$$

where  $G(x, y)$  is the  $2d$ -dimensional Green's function [13] that represents the impulse response of the underlying system subject to homogeneous Dirichlet boundary condition, namely, for any fixed  $x \in \Omega$ ,

$$(2.14) \quad \begin{aligned} -\nabla_y \cdot (c(y)\nabla_y G(x, y)) - k^2(y)G(x, y) &= \delta(y - x), & \text{in } \Omega, \\ G(x, y) &= 0, & \text{on } \partial\Omega. \end{aligned}$$

Here and throughout this work, the subscript in  $\nabla_y$  means differentiation with respect to the  $y$ -variable, and  $\delta(\cdot)$  is the Dirac delta function satisfying  $\delta(z) = 0$  if  $z \neq 0$  and  $\int_R \delta(z) dz = 1$ . Unfortunately, constructing the analytic Green's function for a given domain is in general a difficult matter, which can be built only when the domain geometry and differential operator are simple and regular enough [10]. Besides, numerically solving the equation (2.14) is also not easy because of [34]:

- (1) the dimension of Green's function is twice than that of original problem;
- (2) the computational domain of Green's function may be very complex;
- (3) the singularity of Green's function incurs mathematical difficulties.

More specifically, the first two issues make it impractical to employ the traditional mesh-based approaches, *e.g.*, the finite difference [28] or finite element [8] methods, for solving equation (2.14). As an attractive alternative, the deep learning-based techniques [23] offer distinctive advantages in handling the high-dimensionality and complex geometries.

To handle the singularities caused by  $\delta(\cdot)$ , one class of current methods [14, 6, 32] generates a sufficient number of data pairs  $\{(u_j, f_j)\}_{j=1}^N$  to solve the corresponding optimization problem derived from (2.13), rather than directly solving (2.14). Another class of methods addresses this issue by modifying the original equations (2.14), including using Gaussian functions to approximate the Dirac delta function [44] or fundamental solutions [34] to remove it. These methods reduce the burden of data generation, however, the former approach introduces modeling errors, while the latter fails in cases where the fundamental solution is unknown. Our work addresses this issue in subsection 3.1.

Once the Green's function is obtained via deep learning, referred to as the neural Green's function, its mathematical properties enable a wide range of applications. One clear application is the development of fast-solvers for various types of operators based on (2.13). Furthermore, the discrete approximation of the Green's function, denoted as  $\widehat{B} \in \mathbb{R}^{n \times n}$ , can be employed to construct preconditioners for the GMRES method, since the Green's function represents the continuous form of the inverse stiffness matrix [28], *i.e.*,

$$(2.15) \quad (\widehat{B})_{i,j} \approx G(x_i, x_j) = (A^{-1})_{i,j}, \quad \text{for all } 1 \leq i, j \leq n.$$

Additionally, matrix  $\widehat{B}$  can also be used as an iterator in (2.5) to recover the error vector  $E^{[m]}$  during the  $m$ th iteration. Both theoretical analysis and numerical experiments in subsection 3.3 demonstrate that our training model exhibits a spectral bias of learning components from low to high frequencies. Consequently, employing  $\widehat{B}$  to recover the error vector  $E^{[m]}$  enables rapid convergence for low-frequency components in the error, which contrasts with the smoothing effects of the damped Jacobi method. Based on this, we develop a hybrid iterative method that combines our neural Green's function with the damped Jacobi method to achieve accelerated convergence for all frequency components.

**3. Neural Green's Function.** To alleviate the Dirac delta source term, the original problem (2.14) is reformulated as an interface problem in section 3.1, which is then embedded in a higher-dimensional space to address the jump in the derivative. The solution is obtained through a lift-and-embed learning method, with the algorithm in details presented in section 3.2. Both theoretical analysis and numerical validation of the spectral bias in our training model are conducted in section 3.3, inspiring the development of the following hybrid iterative methods. In section 3.4, we demonstrate the capability of our method to solve indefinite problems involving a piecewise constant coefficient, where the original problem is embedded in a five-dimensional space.

**3.1. Green's Function Embedded in a Higher-dimensional Space.** For the sake of simplicity, we begin by considering the case where the coefficient function  $c(\cdot)$  in (2.1) is smooth and nonzero over the domain  $\Omega$ . In the one-dimensional case, let  $[[\cdot]]$  denote the jump across the given interface  $\Gamma = \{y = x\}$ , and the original problem (2.14) can be reformulated as an interface problem [43], which for any fixed  $x \in \Omega$  is given by

$$(3.1) \quad \begin{aligned} -\nabla_y \cdot (c(y)\nabla_y G(x, y)) - k^2(y)G(x, y) &= 0, & y \in \Omega \setminus \Gamma, \\ G(x, y) &= 0, & y \in \partial\Omega, \\ [[G(x, y)]] &= \lim_{y \rightarrow x^+} G(x, y) - \lim_{y \rightarrow x^-} G(x, y) = 0, & y \in \Gamma, \\ [[\nabla_y G(x, y)]] &= \lim_{y \rightarrow x^+} \nabla_y G(x, y) - \lim_{y \rightarrow x^-} \nabla_y G(x, y) = -c^{-1}(x), & y \in \Gamma. \end{aligned}$$

The Dirac delta function in (2.14) is eliminated through this reformulation. While the continuity of the Green's function on  $\Gamma$  is physically embedded in the neural network architecture, it is challenging for a single neural network to capture the jump in the derivative even with activation functions such as ReLU [45]. To address this issue, we embed problem (3.1) in a lifted higher-dimensional space, where  $G(x, y)$  can be interpreted as the restriction of a newly defined function  $\widehat{G}(x, y, r)$  to a two-dimensional surface, *i.e.*,

$$(3.2) \quad G(x, y) = \widehat{G}(x, y, r(x, y)), \quad \forall x \in \Omega, y \in \Omega \cup \partial\Omega.$$

For notational simplicity, we denote the lifted function as  $\widehat{G}$ , which is smooth in the three-dimensional space, and  $r$  is an augmented variable defined as  $r = r(x, y) = |y - x|$  in order to capture the jump across the interface  $\Gamma$ . Let  $\nabla_y \widehat{G}$  represent the partial derivative of  $\widehat{G}$  with respect to the second  $y$ -variable only, treating  $x, y, r$  as three independent variables, which follows the notation used in [45]. Then the equations

that  $\widehat{G}$  satisfies on the surface for any fixed  $x \in \Omega$  is given by

$$(3.3) \quad \begin{aligned} \widehat{\mathcal{L}}_y \widehat{G}(x, y, r(x, y)) &= 0, & y \in \Omega \setminus \Gamma, \\ \widehat{G}(x, y, r(x, y)) &= 0, & y \in \partial\Omega, \\ 2\partial_r \widehat{G}(x, y, r(x, y)) &= -c^{-1}(x), & y \in \Gamma, \end{aligned}$$

where the operator  $\widehat{\mathcal{L}}_y$  is defined as <sup>1</sup>

$$\widehat{\mathcal{L}}_y \widehat{G} := -\nabla_y c \cdot (\nabla_y \widehat{G} + \frac{(y-x)}{r} \partial_r \widehat{G}) - c(\Delta_y \widehat{G} + \frac{2(y-x)}{r} \cdot \nabla_y (\partial_r \widehat{G}) + \partial_{rr} \widehat{G}) - k^2 \widehat{G}.$$

*Remark 3.1.* Despite the fact that  $\widehat{G}$  is a three-dimensional function, problem (3.3) is still solved on the two-dimensional surface embedded in the lifted space, which will not increase the sampling costs of our following deep learning. As an intuitive illustration, Figure 1 presents the results of solving the one-dimensional Helmholtz equation with the wavenumber  $k = 10$ .

**AN ILLUSTRATIVE EXAMPLE.** *As shown in Figure 1a, sampling only occurs on the 2-dimensional surface which resembles a sharp corner, as determined by the augmented variable  $r = |x - y|$ . After projecting the lifted function onto the original space, we obtain the approximate Green's function depicted in Figure 1b, showing high accuracy with the pointwise error presented in Figure 1c. For a fixed  $y$  ( $y = 0.3$ ), the black curve  $\widehat{G}(x, 0.3, |x - 0.3|)$  shown in Figure 1d is smooth in the 3-dimensional space, while its projection  $\check{G}(x, 0.3)$  depicted in Figure 1e exhibits a jump in its derivative, closely matching the exact Green's function.*

As mentioned above, the continuity of function  $\widehat{G}$  is naturally guaranteed by the use of a single neural network. Although  $\widehat{G}$  only has one value at the interface, the choice of surface determined by the augmented variable  $r = |x - y|$  allows for two distinct values of the derivative at a single point. In fact, our method still works for solving problems involving a discontinuous diffusion coefficient, by embedding the Green's function in a five-dimensional space. For clarity, this topic will be discussed in subsection 3.4.

**3.2. Lift-and-Embed Learning Method.** Even though the lifted function  $\widehat{G}$  brings the curse of the dimensionality, the neural network helps to handle it as follows. The formulas mentioned above help to construct the loss function for training the neural network, which can be effectively resolved using the PINNs [25, 26, 39], deep Ritz method [49], or other deep learning-based methods.

To be precise, the solution ansatz is parametrized using neural networks, *i.e.*,

$$(3.4) \quad \widehat{G}(x, y, r; \theta) = (L_{D_L+1} \circ \sigma \circ L_{D_L} \circ \cdots \circ \sigma \circ L_1 \circ L_0)(x, y, r),$$

where a standard fully-connected neural network [15] with  $D_L \in \mathbb{N}_+$  hidden layers is adopted for implementation. The activation function  $\sigma(\cdot)$  is chosen to be smooth thanks to our lifting operation. The collection of trainable parameters is denoted by  $\theta$  in what follows. The training sets of  $x$  points are generated uniformly at random inside the domain  $\Omega$ , *i.e.*,  $X_\Omega = \{x_n^\Omega\}_{n=1}^{N_\Omega}$ . For each selected  $x$  point, the corresponding sets of  $y$  points are sampled inside the domain  $\Omega$  *i.e.*,  $Y_\Omega = \{y_n^\Omega\}_{n=1}^{N'_\Omega}$ , as well as on the boundary  $\partial\Omega$ , *i.e.*,  $Y_{\partial\Omega} = \{y_n^{\partial\Omega}\}_{n=1}^{N_{\partial\Omega}}$ . Additionally, points are sampled at the

<sup>1</sup>Details of the derivation are provided in the appendix.

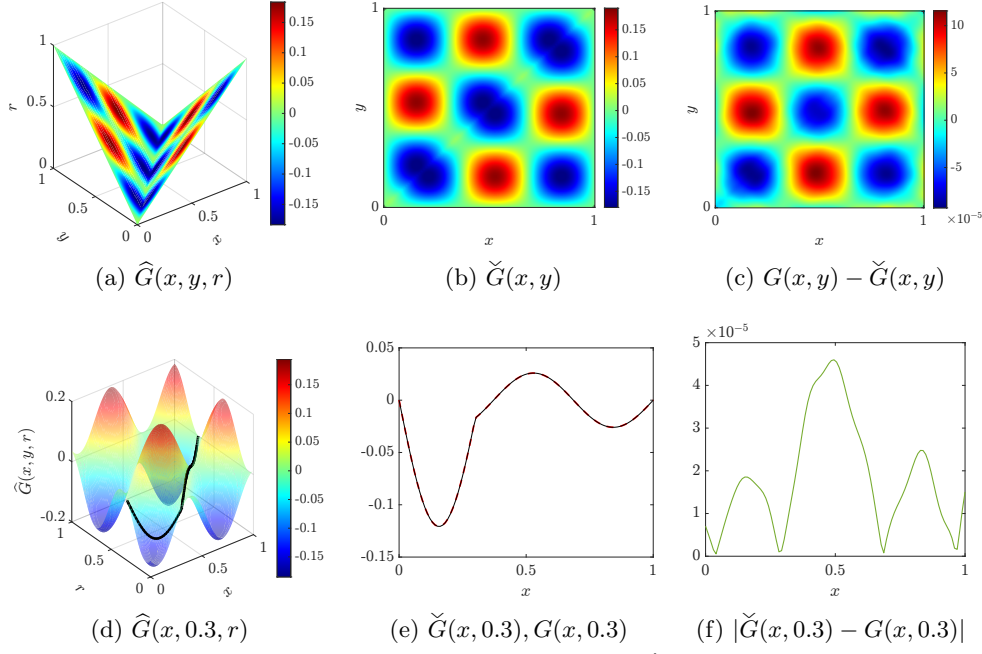


Fig. 1: The first column shows the numerical solution  $\widehat{G}(x, y, r)$  to problem (3.3) on the surface where  $r = |y - x|$  and  $y = 0.3$  respectively. The second column depicts the corresponding projection onto the original space  $\check{G}(x, y)$  in the whole domain and for the fixed  $y$ , approximating the solution to problem (3.1), with the pointwise errors shown in the final column.

interface  $\Gamma$ , *i.e.*,  $X_\Gamma = \{x_n^\Gamma\}_{n=1}^{N_\Gamma}$ . Here  $N_\Omega, N'_\Omega, N_{\partial\Omega}$ , and  $N_\Gamma$  indicate the sample size of corresponding datasets. Then the loss functions can be defined in a residual form of equations:

$$\begin{aligned}
L_{\Omega \setminus \Gamma}(\widehat{G}) &= \frac{1}{N_\Omega} \sum_{n=1}^{N_\Omega} \left( \frac{1}{N'_\Omega} \sum_{n'=1}^{N'_\Omega} \left| \widehat{\mathcal{L}}_y \widehat{G}(x_n^\Omega, y_{n'}^\Omega, r(x_n^\Omega, y_{n'}^\Omega); \theta) \right|^2 \right), \\
L_{\partial\Omega}(\widehat{G}) &= \frac{1}{N_\Omega} \sum_{n=1}^{N_\Omega} \left( \frac{1}{N_{\partial\Omega}} \sum_{n'=1}^{N_{\partial\Omega}} \left| \widehat{G}(x_n^\Omega, y_{n'}^{\partial\Omega}, r(x_n^\Omega, y_{n'}^{\partial\Omega}); \theta) \right|^2 \right), \\
L_\Gamma(\widehat{G}) &= \frac{1}{N_\Gamma} \sum_{n=1}^{N_\Gamma} \left| 2\partial_r \widehat{G}(x_n^\Gamma, x_n^\Gamma, r(x_n^\Gamma, x_n^\Gamma); \theta) + c^{-1}(x_n^\Gamma) \right|^2.
\end{aligned}$$

To enhance the symmetry property of the Green's function [44], an additional loss term is defined as:

$$L_\Omega^{\text{sym}}(\widehat{G}) = \frac{1}{N_\Omega} \sum_{n=1}^{N_\Omega} \left( \frac{1}{N'_\Omega} \sum_{n'=1}^{N'_\Omega} \left| \widehat{G}(x_n^\Omega, y_{n'}^\Omega, r(x_n^\Omega, y_{n'}^\Omega)) - \widehat{G}(y_{n'}^\Omega, x_n^\Omega, r(y_{n'}^\Omega, x_n^\Omega)) \right|^2 \right).$$

As an immediate result, the training tasks associated with problem (3.3) takes on the form

$$(3.5) \quad \theta^* = \arg \min_{\theta} L_{\Omega \setminus \Gamma}(\widehat{G}) + \beta_{\partial\Omega} L_{\partial\Omega}(\widehat{G}) + \beta_\Gamma L_\Gamma(\widehat{G}) + \beta_{\text{sym}} L_\Omega^{\text{sym}}(\widehat{G}),$$

where  $\beta_{\partial\Omega}$ ,  $\beta_{\Gamma}$ ,  $\beta_{\text{sym}} > 0$  are user-defined penalty coefficients. Since it is impossible for the loss term  $L_{\Omega}^{\text{sym}}(\widehat{G})$  to achieve the zero training error, we enforce the symmetric property after the network training is completed. For given  $x, y, r = |y - x|$  as inputs, our neural Green's function is acquired by

$$(3.6) \quad \check{G}(x, y) = \widehat{G}(x, y, |y - x|; \theta^*) = \frac{1}{2}(\widehat{G}(x, y, |y - x|; \theta^*) + \widehat{G}(y, x, |y - x|; \theta^*)).$$

Particularly, the neural Green's function allows us to directly compute the solution  $u(x)$  to problem (2.1) for any new forcing term  $f(x)$ , *i.e.*, employing a numerical quadrature rule

$$(3.7) \quad \hat{u}(x) = \sum_{T_p \in \mathcal{T}_h} \sum_{(\omega_y, y_q) \in I_p} \omega_y f(y_q) \widehat{G}(x, y_q, |y_q - x|; \theta^*),$$

for evaluating the integration (2.13), where  $\mathcal{T}_h$  is a tessellation of domain  $\Omega$  with meshwidth  $h > 0$ , and  $(\omega_y, y_q) \in I_p$  the quadrature weights and points of the  $p$ -th element  $T_p$ . Obviously, formula (3.7) only requires a single forward pass of the trained neural network, which is much more efficient than numerically solving problem (2.1) in an online procedure.

To sum up, the implementation details are presented in algorithm 1, followed by an illustrative example to validate the effectiveness of our proposed method.

---

**Algorithm 1:** Lift-and-Embed Learning Method
 

---

**Input:** Training datasets  $X_{\Omega}$ ,  $Y_{\Omega}$ ,  $X_{\Gamma}$  and  $Y_{\partial\Omega}$ ; network model; given forcing term  $f(x)$ .

**Output:** Neural Green's function  $\check{G}(x, y)$  and approximate solution  $\hat{u}(x)$ .

1 *% Training process*

2 **while** *the maximum number of training epochs is reached* **do**

3     successive relaxation draw mini-batch data uniformly at random from  $X_{\Omega}$ ,  $Y_{\Omega}$ ,  $X_{\Gamma}$  and  $Y_{\partial\Omega}$ ;

4     network training by solving the following optimization problem:

$$\theta^* = \arg \min_{\theta} L_{\Omega \setminus \Gamma}(\widehat{G}) + \beta_{\partial\Omega} L_{\partial\Omega}(\widehat{G}) + \beta_{\Gamma} L_{\Gamma}(\widehat{G}) + \beta_{\text{sym}} L_{\Omega}^{\text{sym}}(\widehat{G});$$

5 **end**

6 *% Testing process*

7 *Load trained model to obtain  $\check{G}(x, y)$  via (3.6) and compute  $\hat{u}(x)$  via (3.7);*

---

AN ILLUSTRATIVE EXAMPLE. *As a direct result, the approximate solution  $\hat{u}(x)$  of problem (2.1) can be immediately obtained using our neural Green's function. The numerical solution using our neural Green's function, with the approximation error depicted in Figure 2.*<sup>2</sup>

**3.3. Spectral Bias of Neural Green's Function.** To gain a deeper understanding of our trained Green's function (3.6), we begin by briefly recalling the expansion theorem [43]

<sup>2</sup>The given forcing term is presented in appendix.

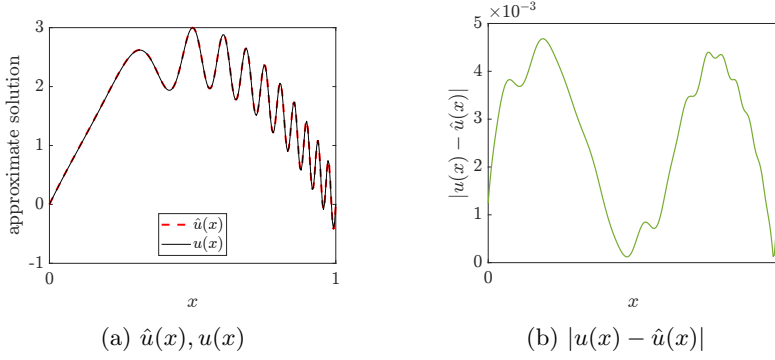


Fig. 2: The exact solution  $u$  and numerical solution  $\hat{u}$  using neural Green's function to problem (2.3), together with the approximation error.

LEMMA 3.2. *Suppose that the symmetric kernel function  $K(x, y) \in L^2(\Omega \times \Omega)$  is continuous and if all but a finite number of eigenvalues are of one sign, then*

$$K(x, y) = \sum_{j=1}^{\infty} \mu_j \phi_j(x) \phi_j(y), \quad \text{uniform on } \Omega \times \Omega,$$

where  $(\mu_j, \phi_j(x))_{j \geq 1}$  is a countable sequence of eigenpairs. Specifically, an indefinite kernel  $K(x, y)$  has a so-called positive decomposition  $K(x, y) = K_+(x, y) + K_-(x, y)$ , where  $K_+$  and  $K_-$  are continuous symmetric positive definite kernels [22]. By applying the Mercer's theorem [21] to each of them, we separate  $(\mu_j, \phi_j(x))_{j \geq 1}$  into two sequences of eigenpairs:  $(\mu_j^+, \phi_j^+(x))_{j \geq 1}$  sort the positive eigenvalues in decreasing order, and  $(\mu_j^-, \phi_j^-(x))_{j \geq 1}$  sort the positive eigenvalues in increasing order [43].

As a direct analogue to the exact Green's function (3.2), the eigenvalue problem associated with the neural Green's function is derived as<sup>3</sup>

$$(3.8) \quad \int_{\Omega} \hat{G}(x, y, r; \theta) \hat{\phi}_j(y) dy = \hat{\mu}_j \hat{\phi}_j(x).$$

As a result of (3.2) and (3.8), when utilizing the Green's function to obtain the solution (2.13), the exact solution  $u$  and its numerical approximation  $\hat{u}$  can be represented through

$$u(x) = \sum_{j=1}^{\infty} \mu_j \left( \int_{\Omega} f(y) \phi_j(y) dy \right) \phi_j(x) \quad \text{and} \quad \hat{u}(x) = \sum_{j=1}^{\infty} \hat{\mu}_j \left( \int_{\Omega} f(y) \hat{\phi}_j(y) dy \right) \hat{\phi}_j(x).$$

In fact, the differential operator  $\mathcal{L}$  and the integral operator  $\mathcal{G}$  share the same eigenfunctions, but the nonzero eigenvalues are reciprocals of each other [43]. Thanks to the learning process of our training model, the dominant eigenmodes (or low-frequency components) of the integral operator  $\mathcal{G}$ , or equivalently, the differential operator  $\mathcal{L}$  could be recovered with high accuracy (to be theoretically and numerically validated later). That is to say, the low-frequency part is of satisfactory accuracy, while the high-frequency part is less precise. Consequently, the approximate solution (3.7) using neural Green's function is always found to seem correct but not good enough to

<sup>3</sup>Note that our neural Green's function is continuous and symmetric by its form of construction (3.6).

convince engineers and scientists to use it. Fortunately, the high-frequency errors can be effectively and efficiently eliminated using the traditional numerical methods [28].

AN ILLUSTRATIVE EXAMPLE. *Note that the eigenproblem associated with problem (2.3) reads*

$$(3.9) \quad \begin{aligned} -\phi_j''(x) - k^2\phi_j(x) &= \mu_j^{-1}\phi_j(x) \quad \text{in } (0, 1), \\ \phi_j(0) &= \phi_j(1) = 0, \end{aligned}$$

for  $j \geq 1$ , where the eigenvalue  $\mu_j^{-1} = j^2\pi^2 - k^2$  corresponds essentially one eigenfunction  $\phi_j(x) = \sqrt{2}\sin(j\pi x)$  [43].

The direct analysis of the spectral bias in the training task (3.5) formulated as a PINN model involves verification of several loss terms, which complicates the proof and remains an open question. To simplify the issue, we consider the following optimization problem for fitting the exact Green's function:

$$(3.10) \quad \theta^* = \arg \min_{\theta} L(\theta) = \arg \min_{\theta} \int_0^1 \int_0^1 \left( \widehat{G}(x, y, r; \theta) - G(x, y) \right)^2 dy dx,$$

where  $\widehat{G}(x, y, r)$  is still parametrized using a standard fully-connected neural network with a smooth activation function  $\sigma(\cdot)$ , as mentioned in (3.4). The extension to  $\Omega = (a, b)$  is easily achieved by applying the substitution method. In order to investigate the spectral bias in the training dynamics related to (3.10), we expand the approximation error during the training process in terms of the orthonormal eigenfunctions:

$$(3.11) \quad \widehat{G}(x, y, r; \theta) - G(x, y) = \sum_{j=1}^{+\infty} \gamma_j(\theta) \phi_j(x) \phi_j(y),$$

with the corresponding coefficient computed by

$$(3.12) \quad \gamma_j(\theta) = \left| \int_0^1 \int_0^1 (\widehat{G}(x, y, r; \theta) - G(x, y)) \phi_j(x) \phi_j(y) dy dx \right|.$$

By defining the  $L^2$  loss over high frequencies  $j \geq \eta$  for our neural approximation as

$$(3.13) \quad L_{\eta^+}(\theta) = \sum_{j=\eta}^{+\infty} \gamma_j^2(\theta),$$

the following theorem demonstrates the spectral bias that our neural Green's function fits the exact one from low to high frequencies. <sup>4</sup> Here we only focus on the interior approximation error, as the Dirichlet boundary condition can be enforced by defining a large penalty coefficient  $\beta_{\partial\Omega}$ .

**THEOREM 3.3** (Spectral bias of neural Green's function fitting the exact  $G(x, y)$ ). *Given the assumptions that*

1. for  $T > 0$ , there is a constant  $c_0 > 0$  such that  $\inf_{t \in (0, T)} |\nabla_{\theta} L(\theta)| \geq c_0$ ,
2.  $\widehat{G}(x, y, r; \theta) = 0$  on  $\partial\Omega$  i.e.,  $\widehat{G}(x, 0, |x|; \theta) = \widehat{G}(x, 1, |x-1|; \theta) = 0$ ,

<sup>4</sup>The proof is provided in the appendix.

then for any  $\eta \geq \frac{k}{\sqrt{\pi^2 - 1}}$  and any  $0 < \delta < 1$ , there exists a constant  $C > 0$  such that

$$(3.14) \quad \frac{|dL_{\eta^+}(\theta)/dt|}{|dL(\theta)/dt|} \leq C\eta^{-(1-\delta)}, \quad \forall t \in (0, T],$$

where  $\widehat{G}(x, y, r; \theta)$  is parametrized using a fully-connected neural network defined in (3.4) with a smooth activation function  $\sigma(\cdot)$ .

*Remark 3.4.* The second assumption that  $\widehat{G}(x, y, r; \theta) = 0$  on  $\partial\Omega$  can be achieved by imposing hard constraints on it [11]. For example, one could define  $\widehat{G}(x, y, r; \theta) := \rho(x, y)\widehat{H}(x, y, r; \theta)$ , where  $\rho(x, y) \in C^\infty(\Omega \times \Omega)$  is a distance function such that  $\rho(x, 0) = \rho(x, 1) = 0$ . A similar proof can be applied.

For further demonstration, we provide numerical validation of the spectral bias related to the learning process (3.5) by numerically solving the eigenvalue problem (3.8), e.g., using the finite element method [12]: given the finite element space  $V_h$  on  $\mathcal{T}_h$ , find  $0 \neq \hat{\mu}_j$  and  $\hat{\phi}_j \in V_h \subset L^2(\Omega)$  such that

$$\int_0^1 \int_0^1 \widehat{G}(x, y, r; \theta) \hat{\phi}_j(y) \varphi(x) dy dx = \hat{\mu}_j \int_0^1 \hat{\phi}_j(x) \varphi(x) dx \quad \text{for any } \varphi(x) \in V_h.$$

The computational results presented in Figure 3<sup>5</sup> demonstrate that the high-frequency eigenvalues of the neural Green's function do not align as closely with the exact ones as the low-frequency eigenvalues do, implying the inherent difficulty for neural networks to learn eigenpairs intensifies with increasing frequencies.

**3.4. Interface Problems with Discontinuous Diffusion Coefficient.** Next, we address a more challenging case with a discontinuous coefficient  $c(\cdot)$  in problem (2.14). Let  $\Omega$  be separated into two subdomains  $\Omega_1 = \{y|y < \alpha, y \in \Omega\}$  and  $\Omega_2 = \{y|y > \alpha, y \in \Omega\}$ , which satisfy  $\overline{\Omega} = \overline{\Omega_1} \cap \overline{\Omega_2}$  while  $\Omega_1 \cap \Omega_2 = \emptyset$ . We consider  $c(\cdot)$  to be a nonzero piecewise constant function, defined as

$$(3.15) \quad c(y) = \begin{cases} c_1, & y \in \Omega_1, \\ c_2, & y \in \Omega_2, \end{cases}$$

which exhibits a finite jump across the interface  $\Sigma = \{y = \alpha\}$ . We also divide the interface  $\Gamma$  defined in (3.1) into  $\Gamma_i = \Omega_i \cap \Gamma$ , for  $i = 1, 2$ . In the one-dimensional case, by removing the  $\delta(x - y)$  as we do when deriving (3.1), the original problem (2.14) for any fixed  $x \in \Omega$ ,  $i = 1, 2$  can be reformulated as [43]:

$$(3.16) \quad \begin{aligned} -\nabla_y \cdot (c(y)\nabla_y G(x, y)) - k^2(y)G(x, y) &= 0, & y \in \Omega_i \setminus \Gamma_i, \\ G(x, y) &= 0, & y \in \partial\Omega, \end{aligned}$$

when  $x \neq \alpha$ , the interface condition on  $\Gamma_i$  ( $y = x \neq \alpha$ ) is rewritten as

$$(3.17) \quad \llbracket G(x, y) \rrbracket = 0 \text{ and } \llbracket \nabla_y G(x, y) \rrbracket = -c_i^{-1}, \quad y \in \Gamma_i,$$

the interface condition on  $\Sigma$  ( $y = \alpha \neq x$ ), introduced by the discontinuity of  $c(\cdot)$ , is rewritten as

$$(3.18) \quad \llbracket G(x, y) \rrbracket = 0 \text{ and } \llbracket c(y)\nabla_y G(x, y) \rrbracket = 0, \quad y \in \Sigma,$$

<sup>5</sup>The details are presented in the appendix.

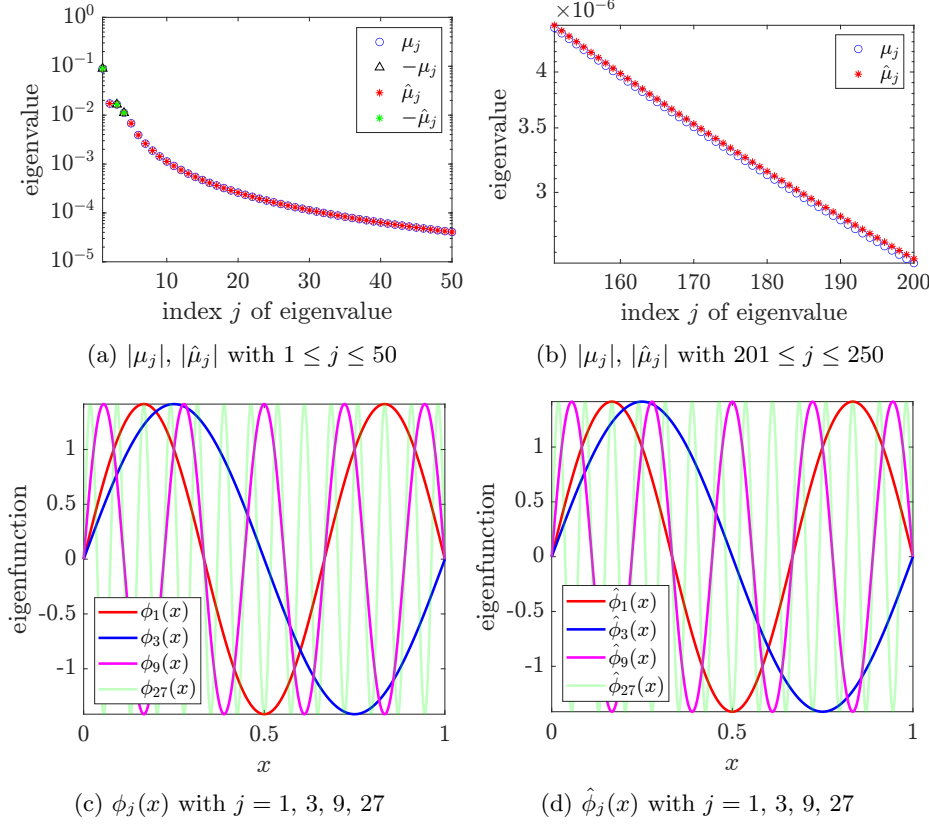


Fig. 3: Eigenpairs computed with neural Green's function for model problem (3.9).

and when  $x = \alpha$ , the two interfaces  $\Gamma$  and  $\Sigma$  coincide ( $y = x = \alpha$ ), we have

$$(3.19) \quad \llbracket G(x, y) \rrbracket = 0 \text{ and } \llbracket c(y) \nabla_y G(x, y) \rrbracket = -1, \quad y \in \Sigma.$$

To enhance the ability of the neural network to represent specific properties of the Green's function, we can incorporate a regularization term derived from the jump in the derivative of with respect to  $x$ -variable at the interface  $\{x = \alpha\} \subset \Omega$ , which is still denoted as  $\Sigma$  for simplicity, *i.e.*, when  $y \neq \alpha$ ,

$$(3.20) \quad \llbracket G(x, y) \rrbracket = 0 \text{ and } \llbracket c(x) \nabla_x G(x, y) \rrbracket = 0, \quad x \in \Sigma.$$

Accordingly, to capture the jumps in the derivative across multiple interfaces  $\Gamma$  and  $\Sigma$ , we embed the original Green's function into a five-dimensional space, *i.e.*,

$$(3.21) \quad G(x, y) = \widehat{G}^\alpha(x, y, r(x, y), s(x), s(y)),$$

where  $r = r(x, y)$  is defined as specified in (3.2),  $s_1 = s(x) = |x - \alpha|$  and  $s_2 = s(y) = |y - \alpha|$  are newly defined augmented variables. For any fixed  $x \in \Omega$ ,  $i = 1, 2$ , the newly defined  $\widehat{G}^\alpha$  satisfies

$$(3.22) \quad \begin{aligned} \widehat{\mathcal{L}}_y^\alpha \widehat{G}^\alpha &= 0, & y \in \Omega_i \setminus \Gamma_i, \\ \widehat{G}^\alpha &= 0, & y \in \partial\Omega, \end{aligned}$$

when  $x \neq \alpha$ ,

$$\begin{aligned} 2\partial_r \widehat{G}^\alpha &= -c_i^{-1}, & y \in \Gamma_i, \\ (c_2 - c_1)(\nabla_y \widehat{G}^\alpha + \frac{y-x}{r} \partial_r \widehat{G}^\alpha) + (c_2 + c_1) \partial_{s_2} \widehat{G}^\alpha &= 0, & y \in \Sigma, \end{aligned}$$

when  $x = \alpha$ ,

$$(c_2 - c_1) \nabla_y \widehat{G}^\alpha + (c_2 + c_1) (\partial_r \widehat{G}^\alpha + \partial_{s_2} \widehat{G}^\alpha) = -1, \quad y \in \Sigma.$$

Here operators  $\widehat{\mathcal{L}}_y^\alpha$  is defined as <sup>6</sup>

$$\begin{aligned} \widehat{\mathcal{L}}_y^\alpha \widehat{G}^\alpha &= -c \left( \Delta_y \widehat{G}^\alpha + \frac{2(y-x)}{r} \nabla_y (\partial_r \widehat{G}^\alpha) + \frac{2(y-\alpha)}{s_2} \nabla_y (\partial_{s_2} \widehat{G}^\alpha) + \partial_{rr} \widehat{G}^\alpha \right. \\ &\quad \left. + \partial_{s_2 s_2} \widehat{G}^\alpha + \frac{2(y-x)(y-\alpha)}{r s_2} \partial_{r s_2} \widehat{G}^\alpha \right) - k^2 \widehat{G}^\alpha. \end{aligned}$$

**4. Neural Green's Function Accelerated Iterative Methods.** It is evident that the discrete approximation of the Green's function  $\widehat{B} \in \mathbb{R}^{n \times n}$ , as presented in (2.15), can be obtained through the forward pass of our neural network *i.e.*,

$$(4.1) \quad (\widehat{B})_{i,j} = \check{G}(x_i, x_j), \text{ for all } 1 \leq i, j \leq n,$$

which subsequently serves as the preconditioner for the linear algebraic system (2.2) in subsection 4.1 and utilized to generate hybrid iterative methods in subsection 4.2.

**4.1. Neural Green's Preconditioner.** The preconditioned system given by

$$(4.2) \quad \widehat{B}AU = \widehat{B}F$$

has the potential to demonstrate improved spectral properties, with the preconditioned GMRES method provided in algorithm 2. Notably, once the neural Green's function is trained, attainment of  $\widehat{B}$  for different mesh sizes  $h$  incurs a minimal cost associated solely with the forward propagation.

---

**Algorithm 2:** Neural Green's function Preconditioned GMRES Method

---

**Input:** The coefficient matrix  $A \in \mathbb{R}^{n \times n}$ ; right-hand side vector  $F \in \mathbb{R}^n$ ; number of total steps  $M$ ; neural Green's function  $\check{G}(x, y)$ .

**Output:** Approximation solution  $U^{[M]} \in \mathbb{R}^n$ .

- 1 Acquire the preconditioner  $\widehat{B} \in \mathbb{R}^{n \times n}$  via (4.1);
  - 2 Initialize the starting vector  $U^{[0]} \in \mathbb{R}^n$  to all zeros;
  - 3 Calculate the initial residual vector  $\widehat{R}^{[0]} = \widehat{B}(F - AU^{[0]})$ ;
  - 4 **for**  $m \leftarrow 0$  **to**  $M - 1$  **do**
  - 5     | update the approximation solution  $U^{[m+1]}$  via the preconditioned GMRES;
  - 6 **end**
- 

AN ILLUSTRATIVE EXAMPLE. *We persist in investigating the problem defined by (2.3), accompanied by the specified forcing term given by (C.2). Here the Generalized Minimal Residual Method (GMRES) is employed to solve the indefinite linear system*

<sup>6</sup>Details of the derivation are provided in the appendix.

(2.2), whose convergence rate is closely linked to the spectral condition number  $\kappa(A)$  defined as

$$(4.3) \quad \kappa(A) := \frac{\lambda_{\max}\lambda_{\min}}{\lambda_s\lambda_{s+1}},$$

where intervals  $[\lambda_{\min}, \lambda_s] \cup [\lambda_{s+1}, \lambda_{\max}]$  contain all eigenvalues of  $A$  with  $\lambda_{\min} < \lambda_s < 0 < \lambda_{s+1} < \lambda_{\max}$  [18].

The original indefinite linear system with a mesh size of  $2^{-8}$  ( $h = 2^{-8}$ ) has a large  $\kappa(A)$  reaching  $2.34 \times 10^4$ . Moreover, as  $h$  decreases,  $\kappa(A)$  grows at the rate  $\mathcal{O}(h^{-1})$ . In contrast, as illustrated in Table 1, the spectral condition number after preconditioning,  $\kappa(\widehat{B}A)$ , grows at a more slow rate and still approaches 1 with the decreasing mesh size. Table 1 also presents the number of iterations required by the GMRES method to achieve the relative residual

$$(4.4) \quad \text{relres} = \frac{\|F - AU^{[m]}\|}{\|F\|},$$

where  $A, F$  has been defined in (2.2), demonstrating the reduced number of iterations after preconditioning. Only small-scale matrices are used for testing here, as with large-scale matrices, the accumulation of round-off errors becomes significant and can not be ignored. More sophisticated techniques are required in such cases, where hierarchical matrices [4] offer data-sparse approximations.

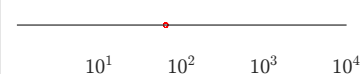
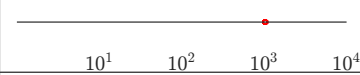
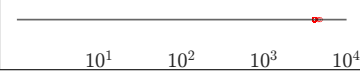
meshsize $h$	eigenvalue $\lambda_j(\widehat{B}A)$	$\kappa(\widehat{B}A)$	iterations	relative residual
$2^{-6}$		1.02	2 (37)	$3.02 \times 10^{-5}$ ( $9.96 \times 10^{-4}$ )
$2^{-8}$		1.01	2 (126)	$1.28 \times 10^{-5}$ ( $9.96 \times 10^{-4}$ )
$2^{-10}$		1.04	3 (1021)	$2.08 \times 10^{-6}$ ( $6.65 \times 10^{-5}$ )
$2^{-12}$		1.17	4 (4083)	$1.06 \times 10^{-6}$ ( $9.96 \times 10^{-5}$ )

Table 1: The effect of our preconditioning, with results of solving the original systems related to (2.3) given within parentheses for comparison.

**4.2. Hybrid Iterative Method.** Recalling the iteration cycle (2.4)-(2.6) for solving the linear system (2.2), the matrix  $\widehat{B}$  obtained from (4.1) can also be applied as the iterator in step (2.5). In our hybrid iterative method, each iteration from  $\widehat{U}^{[m]}$  to  $\widehat{U}^{[m+1]}$  involves one update of the solution reformulated as

$$(4.5) \quad \widehat{U}^{[m+1;0]} = \widehat{U}^{[m]} + \widehat{B}R^{[m]},$$

followed by  $L_\omega$  updates using the damped Jacobi method *i.e.*,

$$\widehat{U}^{[m;\ell+1]} = \left( (1-\omega)I - \omega D^{-1}(\tilde{L} + \tilde{U}) \right) \widehat{U}^{[m;\ell]} + \omega \tilde{D}^{-1}R^{[m;\ell]}, \quad \text{for } 0 \leq \ell \leq L_\omega - 1,$$

where  $\tilde{D}, \tilde{L}, \tilde{U}, \omega$  has been defined in (2.7), and  $R^{[m;\ell]}$  represents the residual at  $\ell$ th Jacobi step. During the  $m$ th iteration, the low-frequency components of the error  $\hat{E}^{[m]}$  are reduced by the use of  $\hat{B}$ , while the high-frequency components are diminished by the damped Jacobi method. The full algorithm is presented in algorithm 3.

---

**Algorithm 3:** Hybrid Iterative Method

---

**Input:** The coefficient matrix  $A \in \mathbb{R}^{n \times n}$ ; right-hand side vector  $F \in \mathbb{R}^n$ ; relaxation factor  $\omega$ ; number of total iterations  $M$ ; number of the Jacobi steps in each iteration  $L_\omega$ ; neural Green's function  $\check{G}(x, y)$ .

**Output:** Approximation solution  $\hat{U}^{[M]} \in \mathbb{R}^n$ .

```

1 Acquire the iterator  $\hat{B} \in \mathbb{R}^{n \times n}$  via (4.1);
2 Initialize the starting vector  $\hat{U}^{[0]} \in \mathbb{R}^n$  to all zeros;
3 for  $m \leftarrow 0$  to  $M - 1$  do
4   calculate the residual vector  $R^{[m]} = F - A\hat{U}^{[m]}$ ;
5    $\hat{U}^{[m;0]} = \hat{U}^{[m]} + \hat{B}R^{[m]}$ ;
6   for  $\ell \leftarrow 0$  to  $L_\omega - 1$  do
7      $R^{[m;\ell]} = F - A\hat{U}^{[m;\ell]}$ ;
8      $\hat{U}^{[m;\ell+1]} = \left( (1 - \omega)I - \omega\tilde{D}^{-1}(\tilde{L} + \tilde{U}) \right) \hat{U}^{[m;\ell]} + \omega\tilde{D}^{-1}R^{[m;\ell]}$ ;
9   end
10  update the solution  $\hat{U}^{[m+1]} = \hat{U}^{[m;L_\omega]}$ ;
11 end
```

---

**AN ILLUSTRATIVE EXAMPLE.** We continue to consider the problem (2.3) with the forcing term specified in (C.2). The numerical solutions achieved by the hybrid iterative method and the pure damped Jacobi Method, with a mesh size of  $2^{-8}$ , are depicted in Figure 4. The parameter  $L_\omega$  is set to 1 for the hybrid iterations, which provides the best performance compared to other values.

The first two rows in Figure 4 demonstrate that our hybrid iterative method converges to machine precision in fewer than 20 iterations for this indefinite problem, whereas the damped Jacobi method remains far away from convergence. The mode-wise errors of all frequencies during the iterations are depicted in the third row, where all of them decay fast during the hybrid iterations and only high-frequency errors decay during the Jacobi iterations. Specifically, mode-wise errors of three distinct frequencies ( $j = 1, 127, 255$ ) are shown in the final row. The lowest frequency error, shown in Figure 4h, exhibits a “staircase” pattern during hybrid iterations, where it drops sharply with each application of  $\hat{B}$  but increases during each Jacobi iteration. As shown in Figure 4i, the two approaches exhibit comparable convergence for the middle frequency components, though the convergence is still faster during hybrid iterations. For the highest frequency, the error illustrated in Figure 4j rises during the application of  $\hat{B}$  and then fast decays during one Jacobi iteration, implying that the high-frequency approximation error introduced by the neural Green's function is diminished by the Jacobi relaxation.

**5. Numerical Experiments.** In this section, we conduct experiments to show effectiveness of our approach in solving the one-dimensional indefinite boundary value problems, with both continuous and piecewise constant diffusion coefficients, neither of which has a known fundamental solution. Throughout the training process, we

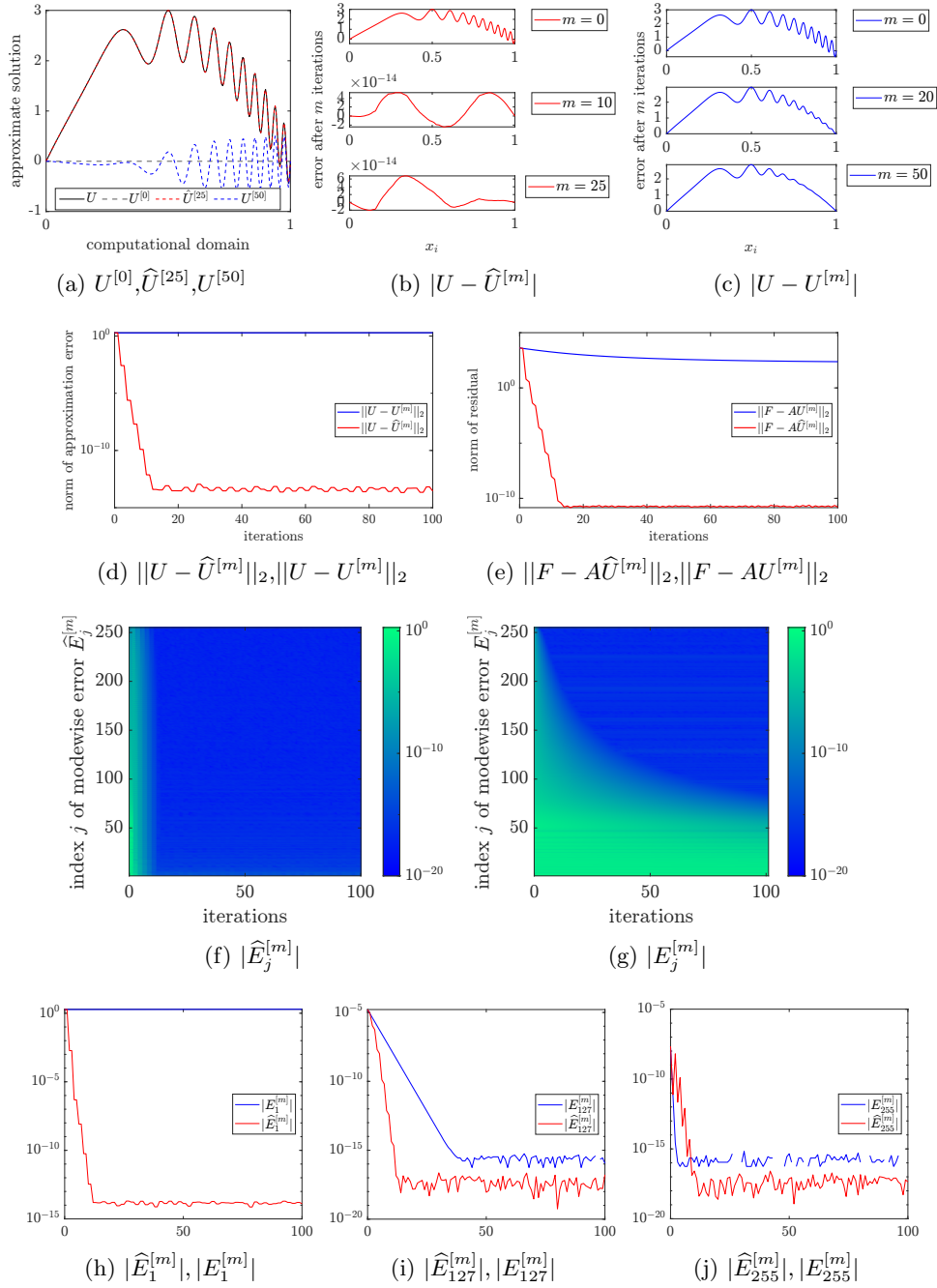


Fig. 4: Approximate solution (a), approximation error (b)(c), norm of the error (d), norm of the residual (e), mode-wise errors of all frequencies (f)(g), and mode-wise errors when  $j = 1, 127, 255$  (h)(i)(j) for solving problem (2.3) through the hybrid iterative method and pure Jacobi method respectively.

employ a fully-connected neural network with a Tanh activation function.

### 5.1. One-dimensional indefinite problem with continuous coefficient.

We first consider the following indefinite problem with a continuous coefficient  $c(x) = (x - 2)^2$  given by

$$(5.1) \quad \begin{aligned} -((x-2)^2 u'(x))' - (15 \sin(10x))^2 u(x) &= f(x), \quad \text{in } (0, 1), \\ u(0) &= u(1) = 0. \end{aligned}$$

Here we employ a neural network consisting of 4 hidden layers, each containing 40 neurons. 500  $x$ -points are randomly selected in  $\Omega$  ( $N_\Omega = 500$ ), and for each  $x$ -point, a corresponding set of 500  $y$ -points is selected in  $\Omega$  and 2  $y$ -points is sampled on  $\partial\Omega$  ( $N'_\Omega = 500, N_{\partial\Omega} = 2$ ). 30,000 points are sampled at the interface  $\Gamma$  ( $N_\Gamma = 30,000$ ). The neural network is trained with parameters set to  $\beta_{\text{sym}} = 400$  and  $\beta_\Gamma = 1000$  for a total of 50,000 epochs. For the first 30,000 epochs, we set the penalty coefficient for the boundary condition to 400 ( $\beta_{\partial\Omega} = 400$ ), and increase it to 4000 ( $\beta_{\partial\Omega} = 4000$ ) for the final 20,000 epochs. The final computational results are presented in Figure 5.

Although the exact Green's function for this problem is not available, we can evaluate the effectiveness of our method by examining the error in recovering  $u$ , with the results presented in Figure 6. After that, the obtained neural Green's function is then utilized to accelerate the corresponding linear algebraic system, which is depicted in Table 2 and Figure 7.

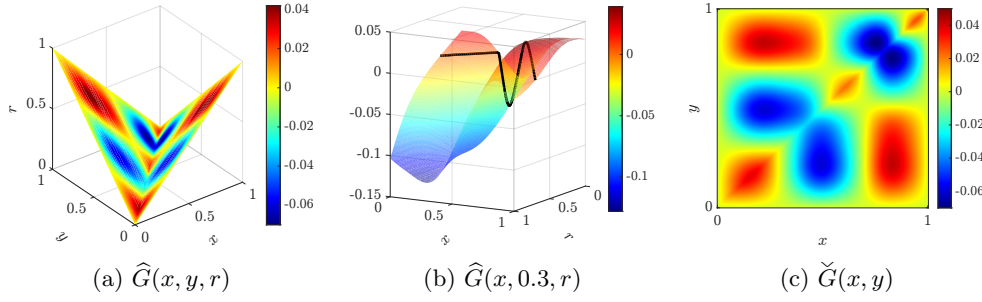


Fig. 5: The numerical solution  $\widehat{G}(x, y, r)$  on the surface where  $r = |x - y|$  and  $y = 0.3$  respectively, together with the projection onto the original space  $\check{G}(x, y)$  for solving (5.1).

**5.2. One-dimensional indefinite problem with a piecewise constant coefficient.** Next, we consider the following indefinite problem with a discontinuous diffusion coefficient:

$$(5.2) \quad \begin{aligned} -(c(x)u'(x))' - k^2 u(x) &= f(x), \quad x \in (-1, 0) \cup (0, 1), \\ u(-1) &= u(1) = 0, \quad x = -1, 1, \\ \llbracket u(x) \rrbracket &= 0 \text{ and } \llbracket [c(x)u'(x)] \rrbracket = 0, \quad x = 0. \end{aligned}$$

where  $k = 10$  and  $c(x)$  is a piecewise constant function

$$(5.3) \quad c(x) = \begin{cases} 1, & x \in (-1, 0), \\ 2, & x \in (0, 1). \end{cases}$$

We use a neural network with 6 hidden layers, each containing 40 neurons, and train it for 20,000 iterations. The sampling parameters are set as  $N_\Omega = N'_\Omega = 80, N_{\partial\Omega} =$

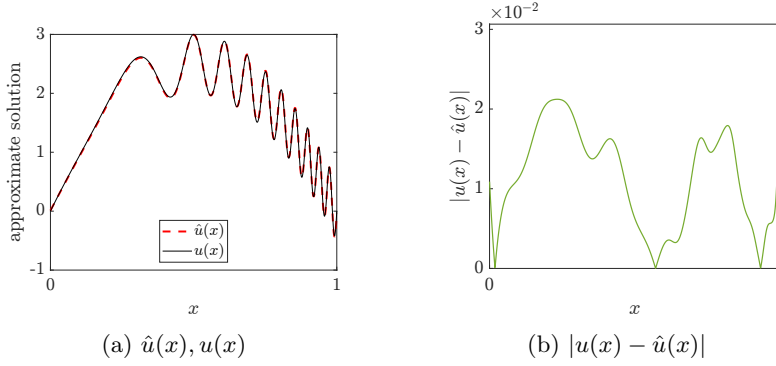


Fig. 6: The exact solution  $u$  and numerical solution  $\hat{u}$  to problem (5.1), together with the approximation error.

meshsize $h$	eigenvalue $\lambda_j(\hat{B}A)$	$\kappa(\hat{B}A)$	iterations	relative residual
$2^{-6}$		1.05	1 (30)	$3.34 \times 10^{-3}$ ( $9.34 \times 10^{-3}$ )
$2^{-8}$		1.33	3 (252)	$5.23 \times 10^{-5}$ ( $5.15 \times 10^{-4}$ )
$2^{-10}$		2.86	4 (1014)	$8.90 \times 10^{-5}$ ( $9.54 \times 10^{-5}$ )
$2^{-12}$		14.82	5 (4058)	$3.03 \times 10^{-6}$ ( $8.97 \times 10^{-5}$ )

Table 2: The effect of our preconditioning, with results of solving the original systems related to (5.1) given within parentheses for comparison.

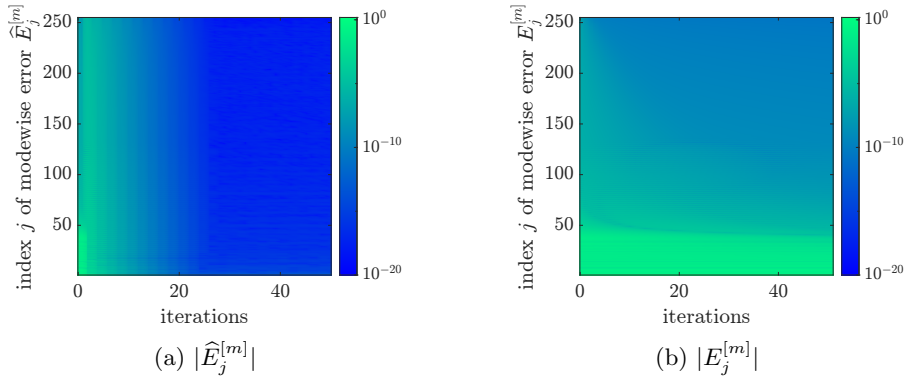


Fig. 7: Mode-wise errors of all frequencies for solving problem (5.1) through the hybrid iterative method and pure Jacobi method respectively.

2, and  $N_\Gamma = N_\Sigma = N_\alpha = 1000$ . The boundary is divided into two parts, where  $\partial_1\Omega := \{(x, -1) | -1 \leq x \leq 0\} \cup \{(-1, y) | -1 \leq y \leq 0\}$  and  $\partial_2\Omega = \partial\Omega \setminus \partial_1\Omega$ , with corresponding penalty coefficients  $\beta_{\partial_1\Omega} = 400$  and  $\beta_{\partial_2\Omega} = 800$ , which are proportional to the scaling of  $c(x)$  in each subdomain. Other penalty coefficients are configured as  $\beta_{\Gamma_i} = \beta_\gamma = \beta_{\text{sym}} = 400$ , for  $i = 1, 2$ . Our neural Green's function is illustrated in Figure 8, and used to recover the solution  $u$  from the forcing term given by

$$(5.4) \quad f(x) = \begin{cases} -100x^3 - 200x^2 - 106x - 4, & x \in (-1, 0), \\ -50x^3 + 100x^2 - 56x + 4, & x \in (0, 1), \end{cases}$$

Results of the iterative methods accelerated by our neural Green's function are presented in Table 2 and Figure 9 respectively.

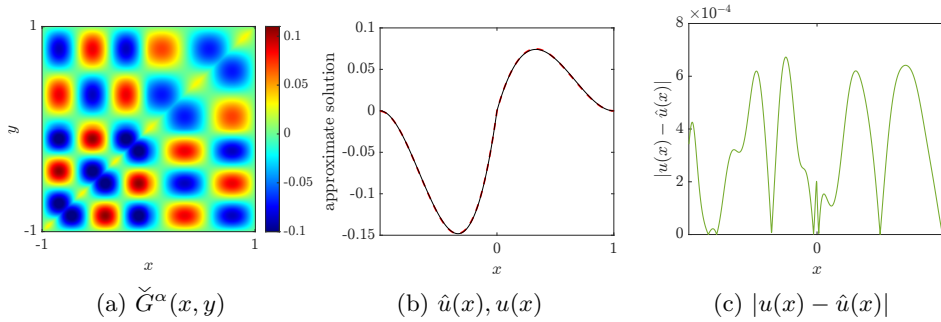


Fig. 8: The projection onto the original space  $\check{G}^\alpha(x, y)$  for solving (5.2), the exact solution  $u$  and numerical solution  $\hat{u}$ , together with the approximation error.

meshsize $h$	eigenvalue $\lambda_j(\hat{B}A)$	$\kappa(\hat{B}A)$	iterations	relative residual
$2^{-6}$		1.10	2 (60)	$8.13 \times 10^{-4}$ ( $6.12 \times 10^{-3}$ )
$2^{-8}$		1.34	3 (246)	$6.85 \times 10^{-4}$ ( $9.55 \times 10^{-4}$ )
$2^{-10}$		1.81	5 (1008)	$9.10 \times 10^{-5}$ ( $9.90 \times 10^{-5}$ )
$2^{-12}$		2.14	8 (4039)	$9.55 \times 10^{-6}$ ( $9.47 \times 10^{-5}$ )

Table 3: The effect of our preconditioning, with results of solving the original systems related to (5.2) given within parentheses for comparison.

**6. Conclusion.** We have developed the neural Green's function, a physics informed neural operator designed to learn the kernel for solving boundary value problems with reduced training data demands. Our approach is effective for solving one-dimensional indefinite problems, even when the coefficient is discontinuous. The governing equations for the Green's function is rewritten into an interface problem to remove the singular Dirac-delta source term. To address the jump in the derivative, this

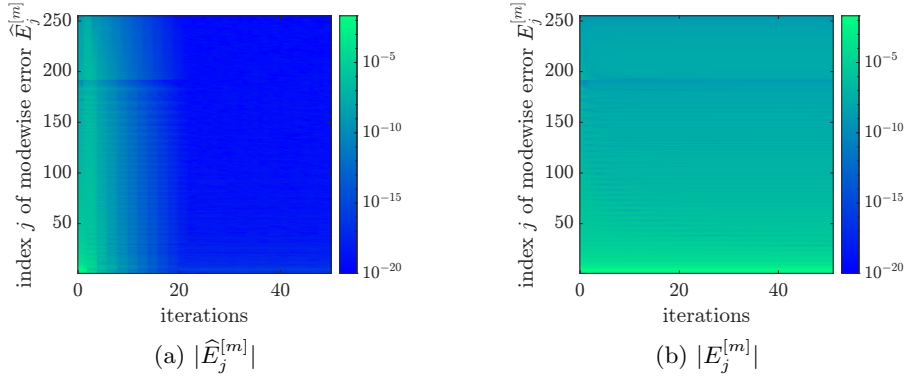


Fig. 9: Mode-wise errors of all frequencies for solving problem (5.2) through the hybrid iterative method and pure Jacobi method respectively.

interface problem is embedded in a lifted space of 3-dimensional when the coefficient is continuous and 5-dimensional when the coefficient exhibits a jump discontinuity. Employment of a single neural network to solve this lifted problem overcomes the curse of the dimensionality and naturally ensures the continuity through its physical architecture. Importantly, sampling costs do not increase, as the lifted problem is still solved on a 2-dimensional surface. In addition to developing fast solvers, the gained neural Green's function is utilized to speed up traditional iterative methods by generating preconditioners for the linear systems. Furthermore, supported by the physics embedded in the kernel, we have conducted a theoretical analysis of the spectral bias in our training model, which progressively recovers the frequency components of the kernel from low to high, in contrast to the smoothing effects of the traditional iterative methods. Consequently, we propose a hybrid iterative solver that combines our neural operator with the damped Jacobi method to achieve fast convergence across all frequency components, even when solving indefinite problems. The effectiveness of iterative methods accelerated by our neural Green function is demonstrated through numerical experiments on various indefinite problems, involving both continuous and piecewise constant coefficients.

Future work includes extending the current one-dimensional framework to higher dimensions, where handling the singularities of Dirac-delta functions becomes more challenging. Additionally, constructing preconditioners and hybrid iterative solvers for large-scale matrices may encounter sparsity and storage issues, which we aim to address by using hierarchical matrices to provide data-sparse approximations. Finally, while the spectral bias for fitting the kernel has been proved, we plan to provide a proof of the spectral bias for the original training task formulated as a PINN model.

## REFERENCES

- [1] W. E. ARNOLDI, *The principle of minimized iterations in the solution of the matrix eigenvalue problem*, Quarterly of applied mathematics, 9 (1951), pp. 17–29.
- [2] K. AZIZZADENESHELI, N. KOVACHKI, Z. LI, M. LIU-SCHIAFFINI, J. KOSSAIFI, AND A. ANANDKUMAR, *Neural operators for accelerating scientific simulations and design*, Nature Reviews Physics, (2024), pp. 1–9.
- [3] Y. AZULAY AND E. TREISTER, *Multigrid-augmented deep learning preconditioners for the helmholtz equation*, SIAM Journal on Scientific Computing, (2022), pp. S127–S151.
- [4] M. BEBENDORF, *Hierarchical matrices*, Springer, 2008.
- [5] B. E. BOSER, I. M. GUYON, AND V. N. VAPNIK, *A training algorithm for optimal margin*

- classifiers*, in Proceedings of the fifth annual workshop on Computational learning theory, 1992, pp. 144–152.
- [6] N. BOULLÉ, C. J. EARLS, AND A. TOWNSEND, *Data-driven discovery of green's functions with human-understandable deep learning*, Scientific reports, 12 (2022), p. 4824.
- [7] N. BOULLÉ AND A. TOWNSEND, *A mathematical guide to operator learning*, arXiv preprint arXiv:2312.14688, (2023).
- [8] S. C. BRENNER AND L. R. SCOTT, *The mathematical theory of finite element methods*, vol. 3, Springer, 2008.
- [9] K. BURRAGE AND J. ERHEL, *On the performance of various adaptive preconditioned gmres strategies*, Numerical linear algebra with applications, 5 (1998), pp. 101–121.
- [10] L. C. EVANS, *Partial Differential Equations*, vol. 19, American Mathematical Society, 2010.
- [11] R. FLETCHER, *Practical methods of optimization*, John Wiley & Sons, 2000.
- [12] P. FRAUENFELDER, C. SCHWAB, AND R. A. TODOR, *Finite elements for elliptic problems with stochastic coefficients*, Computer methods in applied mechanics and engineering, 194 (2005), pp. 205–228.
- [13] D. GILBARG, N. S. TRUDINGER, D. GILBARG, AND N. TRUDINGER, *Elliptic partial differential equations of second order*, vol. 224, Springer, 1977.
- [14] C. R. GIN, D. E. SHEA, S. L. BRUNTON, AND J. N. KUTZ, *Deepgreen: deep learning of green's functions for nonlinear boundary value problems*, Scientific reports, 11 (2021), p. 21614.
- [15] I. GOODFELLOW, Y. BENGIO, AND A. COURVILLE, *Deep learning*, MIT Press, 2016.
- [16] S. GOSWAMI, A. BORA, Y. YU, AND G. E. KARNIADAKIS, *Physics-informed deep neural operator networks*, in Machine Learning in Modeling and Simulation: Methods and Applications, Springer, 2023, pp. 219–254.
- [17] M. GÖTZ AND H. ANZT, *Machine learning-aided numerical linear algebra: Convolutional neural networks for the efficient preconditioner generation*, in 2018 IEEE/ACM 9th Workshop on Latest Advances in Scalable Algorithms for Large-Scale Systems (scalA), IEEE, 2018, pp. 49–56.
- [18] A. GREENBAUM, *Iterative methods for solving linear systems*, SIAM, 1997.
- [19] J. HAN, A. JENTZEN, AND W. E, *Solving high-dimensional partial differential equations using deep learning*, Proceedings of the National Academy of Sciences, 115 (2018), pp. 8505–8510.
- [20] K. HORNIK, M. STINCHCOMBE, AND H. WHITE, *Multilayer feedforward networks are universal approximators*, Neural networks, 2 (1989), pp. 359–366.
- [21] T. HSING AND R. EUBANK, *Theoretical foundations of functional data analysis, with an introduction to linear operators*, vol. 997, John Wiley & Sons, 2015.
- [22] S. JEONG AND A. TOWNSEND, *Extending mercer's expansion to indefinite and asymmetric kernels*, arXiv preprint arXiv:2409.16453, (2024).
- [23] G. E. KARNIADAKIS, I. G. KEVREKIDIS, L. LU, P. PERDIKARIS, S. WANG, AND L. YANG, *Physics-informed machine learning*, Nature Reviews Physics, 3 (2021), pp. 422–440.
- [24] N. KOVACHKI, Z. LI, B. LIU, K. AZIZZADENESHELI, K. BHATTACHARYA, A. STUART, AND A. ANANDKUMAR, *Neural operator: Learning maps between function spaces*, arXiv preprint arXiv:2108.08481, (2021).
- [25] I. E. LAGARIS, A. LIKAS, AND D. I. FOTIADIS, *Artificial neural networks for solving ordinary and partial differential equations*, IEEE transactions on neural networks, 9 (1998), pp. 987–1000.
- [26] I. E. LAGARIS, A. C. LIKAS, AND D. G. PAPAGEORGIOU, *Neural-network methods for boundary value problems with irregular boundaries*, IEEE Transactions on Neural Networks, 11 (2000), pp. 1041–1049.
- [27] S. LANTHALER, S. MISHRA, AND G. E. KARNIADAKIS, *Error estimates for deep neural networks: A deep learning framework in infinite dimensions*, Transactions of Mathematics and Its Applications, 6 (2022), p. tnac001.
- [28] R. J. LEVEQUE, *Finite difference methods for ordinary and partial differential equations: steady-state and time-dependent problems*, SIAM, 2007.
- [29] Y. LI, P. Y. CHEN, W. MATUSIK, ET AL., *Learning preconditioner for conjugate gradient pde solvers*, arXiv preprint arXiv:2305.16432, (2023).
- [30] Z. LI AND K. ITO, *The immersed interface method: numerical solutions of PDEs involving interfaces and irregular domains*, SIAM, 2006.
- [31] Z. LI, N. KOVACHKI, K. AZIZZADENESHELI, B. LIU, K. BHATTACHARYA, A. STUART, AND A. ANANDKUMAR, *Fourier neural operator for parametric partial differential equations*, arXiv preprint arXiv:2010.08895, (2020).
- [32] Z. LI, N. KOVACHKI, K. AZIZZADENESHELI, B. LIU, K. BHATTACHARYA, A. STUART, AND A. ANANDKUMAR, *Neural operator: Graph kernel network for partial differential equations*, arXiv preprint arXiv:2003.03485, (2020).

- [33] Z. LI, H. ZHENG, N. KOVACHKI, D. JIN, H. CHEN, B. LIU, K. AZIZZADENESHELI, AND A. ANANDKUMAR, *Physics-informed neural operator for learning partial differential equations*, ACM/JMS Journal of Data Science, 1 (2024), pp. 1–27.
- [34] G. LIN, P. HU, F. CHEN, X. CHEN, J. CHEN, J. WANG, AND Z. SHI, *Binet: learning to solve partial differential equations with boundary integral networks*, arXiv preprint arXiv:2110.00352, (2021).
- [35] L. LU, P. JIN, G. PANG, Z. ZHANG, AND G. E. KARNIADAKIS, *Learning nonlinear operators via deepnet based on the universal approximation theorem of operators*, Nature machine intelligence, 3 (2021), pp. 218–229.
- [36] L. LU, X. MENG, S. CAI, Z. MAO, S. GOSWAMI, Z. ZHANG, AND G. E. KARNIADAKIS, *A comprehensive and fair comparison of two neural operators (with practical extensions) based on fair data*, Computer Methods in Applied Mechanics and Engineering, 393 (2022), p. 114778.
- [37] G. PANG, M. D'ELIA, M. PARKS, AND G. E. KARNIADAKIS, *npinns: nonlocal physics-informed neural networks for a parametrized nonlocal universal laplacian operator. algorithms and applications*, Journal of Computational Physics, 422 (2020), p. 109760.
- [38] N. RAHAMAN, A. BARATIN, D. ARPIT, F. DRAXLER, M. LIN, F. HAMPRECHT, Y. BENGIO, AND A. COURVILLE, *On the spectral bias of neural networks*, in International conference on machine learning, PMLR, 2019, pp. 5301–5310.
- [39] M. RAISSI, P. PERDIKARIS, AND G. E. KARNIADAKIS, *Physics-informed neural networks: A deep learning framework for solving forward and inverse problems involving nonlinear partial differential equations*, Journal of Computational physics, 378 (2019), pp. 686–707.
- [40] Y. SAAD AND M. H. SCHULTZ, *Gmres: A generalized minimal residual algorithm for solving nonsymmetric linear systems*, SIAM Journal on scientific and statistical computing, 7 (1986), pp. 856–869.
- [41] Y. SAAD AND H. A. VAN DER VORST, *Iterative solution of linear systems in the 20th century*, Journal of Computational and Applied Mathematics, 123 (2000), pp. 1–33.
- [42] B. SCHÖLKOPF AND A. J. SMOLA, *Learning with kernels: support vector machines, regularization, optimization, and beyond*, MIT press, 2002.
- [43] I. STAKGOLD AND M. J. HOLST, *Green's functions and boundary value problems*, John Wiley & Sons, 2011.
- [44] Y. TENG, X. ZHANG, Z. WANG, AND L. JU, *Learning green's functions of linear reaction-diffusion equations with application to fast numerical solver*, in Mathematical and Scientific Machine Learning, PMLR, 2022, pp. 1–16.
- [45] Y.-H. TSENG, T.-S. LIN, W.-F. HU, AND M.-C. LAI, *A cusp-capturing pinn for elliptic interface problems*, Journal of Computational Physics, 491 (2023), p. 112359.
- [46] S. WANG, H. WANG, AND P. PERDIKARIS, *Learning the solution operator of parametric partial differential equations with physics-informed deepnets*, Science advances, 7 (2021), p. eabi8605.
- [47] Z.-Q. J. XU, Y. ZHANG, T. LUO, Y. XIAO, AND Z. MA, *Frequency principle: Fourier analysis sheds light on deep neural networks*, arXiv preprint arXiv:1901.06523, (2019).
- [48] Z.-Q. J. XU, Y. ZHANG, AND Y. XIAO, *Training behavior of deep neural network in frequency domain*, in Neural Information Processing: 26th International Conference, ICONIP 2019, Sydney, NSW, Australia, December 12–15, 2019, Proceedings, Part I 26, Springer, 2019, pp. 264–274.
- [49] B. YU ET AL., *The deep Ritz method: a deep learning-based numerical algorithm for solving variational problems*, Communications in Mathematics and Statistics, 6 (2018), pp. 1–12.
- [50] E. ZHANG, A. KAHANA, E. TURKEL, R. RANADE, J. PATHAK, AND G. E. KARNIADAKIS, *A hybrid iterative numerical transferable solver (hints) for pdes based on deep operator network and relaxation methods*, arXiv preprint arXiv:2208.13273, (2022).

## Appendix A. Derivation of the Lifted Equations.

### A.1. Derivation of (3.3).

*Proof.* Recalling the definition  $r = |y - x|$  with the derivative given by

$$(A.1) \quad \nabla_y r = \frac{y - x}{r}, \quad \Delta_y r = 0, \quad y \neq x,$$

we can obtain that, when  $y \neq x$ ,

$$\begin{aligned}
\nabla_y G &= \nabla_y \widehat{G} + \nabla_{yr} \partial_r \widehat{G} = \nabla_y \widehat{G} + \partial_r \widehat{G} \frac{y-x}{r} \\
\Delta_y G &= \nabla_y \cdot (\nabla_y \widehat{G} + \partial_r \widehat{G} \nabla_y r) \\
&= \Delta_y \widehat{G} + 2\nabla_y (\partial_r \widehat{G}) \cdot \nabla_y r + (\nabla_y r)^2 \partial_{rr} \widehat{G} + \partial_r \widehat{G} \Delta_y r \\
&= \Delta_y \widehat{G} + 2\nabla_y (\partial_r \widehat{G}) \cdot \frac{y-x}{r} + \partial_{rr} \widehat{G}.
\end{aligned}
\tag{A.2}$$

Substituting (A.2) into the operator  $\mathcal{L}_y$  in (2.14), we have

$$\begin{aligned}
\mathcal{L}_y G &= -\nabla_y \cdot (c \nabla_y G) - k^2 G \\
&= -\nabla_y c \cdot \nabla_y G - c \Delta_y G - k^2 G \\
&= -\nabla_y c \cdot (\nabla_y \widehat{G} + \partial_r \widehat{G} \frac{y-x}{r}) - c (\Delta_y \widehat{G} + 2\nabla_y (\partial_r \widehat{G}) \cdot \frac{y-x}{r} + \partial_{rr} \widehat{G}) - k^2 \widehat{G},
\end{aligned}
\tag{A.3}$$

which is denoted as  $\widehat{\mathcal{L}}_y \widehat{G}$ . Furthermore, because of the continuity of  $\nabla_y \widehat{G}$ ,  $\partial_r \widehat{G}$  and the jump  $[[\nabla_y r]] = 2$  at  $y = x$ , the interface condition is reformulated as

$$[[\nabla_y G]] = \partial_r \widehat{G} [[\nabla_y r]] = 2\partial_r \widehat{G} = -c^{-1}. \quad \square
\tag{A.4}$$

**A.2. Derivation of (3.22).** Similarly, recalling the definitions  $s_1 = |x - \alpha|$  and  $s_2 = |y - \alpha|$ , whose derivatives are calculated by

$$\nabla_y s_1 = \frac{x - \alpha}{s_1}, \quad \nabla_y s_2 = \frac{y - \alpha}{s_2}, \quad \Delta_y s_1 = \Delta_y s_2 = 0, \quad y \neq x, \alpha,
\tag{A.5}$$

we can obtain the derivatives when  $y \neq x, \alpha$ ,

$$\begin{aligned}
\nabla_y G &= \nabla_y \widehat{G}^\alpha + \partial_r \widehat{G}^\alpha \frac{y-x}{r} + \partial_{s_2} \widehat{G}^\alpha \frac{y-\alpha}{s_2}, \\
\Delta_y G &= \Delta_y \widehat{G}^\alpha + \frac{2(y-x)}{r} \cdot \nabla_y (\partial_r \widehat{G}^\alpha) + \frac{2(y-\alpha)}{s_2} \cdot \nabla_y (\partial_{s_2} \widehat{G}^\alpha) + \partial_{rr} \widehat{G}^\alpha \\
&\quad + \frac{2(y-x) \cdot (y-\alpha)}{r s_2} \partial_{r s_2} \widehat{G}^\alpha + \partial_{s_2 s_2} \widehat{G}^\alpha.
\end{aligned}
\tag{A.6}$$

When the coefficient function is defined as (3.15), we have  $\nabla c(y) = 0$  for  $y \neq \alpha$ , and the corresponding operator is reformulated as

$$\begin{aligned}
\mathcal{L}_y G &= -c \nabla_y G - k^2 G \\
&= -c \left( \Delta_y \widehat{G}^\alpha + \frac{2(y-x)}{r} \cdot \nabla_y (\partial_r \widehat{G}^\alpha) + \frac{2(y-\alpha)}{s_2} \cdot \nabla_y (\partial_{s_2} \widehat{G}^\alpha) + \partial_{rr} \widehat{G}^\alpha \right. \\
&\quad \left. + \frac{2(y-x) \cdot (y-\alpha)}{r s_2} \partial_{r s_2} \widehat{G}^\alpha + \partial_{s_2 s_2} \widehat{G}^\alpha \right) - k^2 \widehat{G}^\alpha,
\end{aligned}
\tag{A.7}$$

Note that  $\nabla_y \widehat{G}^\alpha$ ,  $\partial_r \widehat{G}^\alpha$  and  $\partial_{s_2} \widehat{G}^\alpha$  are continuous in the entire domain. When it comes to the interface condition (3.17) at  $y = x \neq \alpha$ ,  $\nabla_y s_2$  is continuous and  $[[\nabla_y r]] = 2$ . Thus we still have

$$[[\nabla_y G]] = \partial_r \widehat{G}^\alpha [[\nabla_y r]] = 2\partial_r \widehat{G}^\alpha = -c_i^{-1}.
\tag{A.8}$$

At the interface  $y = \alpha \neq x$ ,  $\nabla_y r$  is continuous while  $\llbracket c(y)\nabla_y s_2 \rrbracket = c_2 + c_1$ . Then the condition (3.18) is rewritten as

$$(A.9) \quad \llbracket c(y)\nabla_y G \rrbracket = (c_2 - c_1)(\nabla_y \widehat{G}^\alpha + \partial_r \widehat{G}^\alpha \frac{y-x}{r}) + (c_2 + c_1)\partial_{s_2} \widehat{G}^\alpha = 0.$$

Similarly, at  $y = x = \alpha$ , where  $\llbracket c(y)\nabla_y r \rrbracket = \llbracket c(y)\nabla_y s_2 \rrbracket = c_2 + c_1$ , the interface condition (3.19) is reformulated as

$$(A.10) \quad \llbracket c(y)\nabla_y G \rrbracket = (c_2 - c_1)\nabla_y \widehat{G}^\alpha + (c_2 + c_1)(\partial_r \widehat{G}^\alpha \frac{y-x}{r} + \partial_{s_2} \widehat{G}^\alpha) = -1.$$

**Appendix B. Lift-and-Embed Learning Method for Solving Interface Problems with a Discontinuous Diffusion Coefficient.** For simplicity, we use the notation  $\widehat{G}^\alpha(x, y, r, s_1, s_2)$  to represent the solution  $\widehat{G}^\alpha$  to problem (3.22) is parametrized by a single neural network, *i.e.*,  $\widehat{G}^\alpha(x, y, r, s_1, s_2; \theta)$ , ensuring the continuity of the function across all interfaces. Although the function  $\widehat{G}^\alpha$  is 5-dimensional, the sampling is still performed on the 2-dimensional surface. We begin by sampling sets of  $x$ ,  $X_\Omega = \{x_n^\Omega\}_{n=1}^{N_\Omega}$  in  $\Omega \setminus \Sigma$ , along with corresponding sets of  $y$ ,  $Y_\Omega = \{y_{n'}^\Omega\}_{n'=1}^{N'_\Omega}$  in  $\Omega$ , and  $Y_{\partial\Omega} = \{y_{n'}^{\partial\Omega}\}_{n'=1}^{N'_{\partial\Omega}}$  on  $\partial\Omega$  respectively. In each subdomain  $\Omega_i$ ,  $X_{\Gamma_i} = \{x_n^{\Gamma_i}\}_{n=1}^{N_{\Gamma_i}}$  are sampled with the same  $y$  points to satisfy the interface conditions on  $\Gamma$ . For the interface condition on  $\Sigma$ , we sample  $X_\Sigma = \{x_n^\Sigma\}_{n=1}^{N_\Sigma}$  in  $\Omega \setminus (\Gamma \cup \Sigma)$  with corresponding values of  $y$  being  $\{\alpha\}_{i=1}^{N_\Sigma}$ . Similarly,  $Y_\Sigma = \{y_n^\Sigma\}_{n=1}^{N_\Sigma}$  are sampled in  $\Omega \setminus \Sigma$  with corresponding values of  $x$  being  $\{\alpha\}_{i=1}^{N_\Sigma}$ . Finally, we sample  $\{(\alpha, \alpha)\}_{i=1}^{N_\alpha}$  for the interface condition at  $y = x = \alpha$ . The final loss terms are defined as

$$\begin{aligned} L_\Omega(\widehat{G}^\alpha) &= \frac{1}{N_\Omega} \sum_{n=1}^{N_\Omega} \left( \frac{1}{N'_\Omega} \sum_{n'=1}^{N'_\Omega} \left| \widehat{\mathcal{L}}_y^\alpha \widehat{G}^\alpha \left( x_n^\Omega, y_{n'}^\Omega, r(x_n^\Omega, y_{n'}^\Omega), s_1(x_n^\Omega), s_2(y_{n'}^\Omega) \right) \right|^2 \right), \\ L_{\partial\Omega}(\widehat{G}^\alpha) &= \frac{1}{N_\Omega} \sum_{n=1}^{N_\Omega} \left( \frac{1}{N'_{\partial\Omega}} \sum_{n'=1}^{N'_{\partial\Omega}} \left| \widehat{G}^\alpha \left( x_n^\Omega, y_{n'}^{\partial\Omega}, r(x_n^\Omega, y_{n'}^{\partial\Omega}), s_1(x_n^\Omega), s_2(y_{n'}^{\partial\Omega}) \right) \right|^2 \right), \\ L_{\Gamma_i}(\widehat{G}^\alpha) &= \frac{1}{N_{\Gamma_i}} \sum_{n=1}^{N_{\Gamma_i}} \left| 2\partial_r \widehat{G}^\alpha \left( x_n^{\Gamma_i}, x_n^{\Gamma_i}, r(x_n^{\Gamma_i}, x_n^{\Gamma_i}), s_1(x_n^{\Gamma_i}), s_2(x_n^{\Gamma_i}) \right) + c_i^{-1} \right|^2, \\ L_\Sigma(\widehat{G}^\alpha) &= \frac{1}{N_\Sigma} \sum_{n=1}^{N_\Sigma} \left| \Lambda_y \widehat{G}^\alpha \left( x_n^\Sigma, \alpha, r(x_n^\Sigma, \alpha), s_1(x_n^\Sigma), 0 \right) \right|^2, \\ L_\Sigma^*(\widehat{G}^\alpha) &= \frac{1}{N_\Sigma} \sum_{n=1}^{N_\Sigma} \left| \Lambda_x \widehat{G}^\alpha \left( \alpha, x_n^\Sigma, r(\alpha, x_n^\Sigma), 0, s_2(x_n^\Sigma) \right) \right|^2, \\ L_\alpha(\widehat{G}^\alpha) &= \frac{1}{N_\alpha} \sum_{n=1}^{N_\alpha} \left| \Lambda_y \widehat{G}^\alpha \left( \alpha, \alpha, 0, 0, 0 \right) + 1 \right|^2, \end{aligned}$$

where the operators  $\Lambda_y, \Lambda_x$  are defined as

$$\begin{aligned} \Lambda_y \widehat{G}^\alpha &= (c_2 - c_1)\nabla_y \widehat{G}^\alpha + (c_2 + c_1)(\partial_r \widehat{G}^\alpha \frac{y-x}{r} + \partial_{s_2} \widehat{G}^\alpha), \\ \Lambda_x \widehat{G}^\alpha &= (c_2 - c_1)\nabla_y \widehat{G}^\alpha + (c_2 + c_1)(\partial_r \widehat{G}^\alpha \frac{y-x}{r} + \partial_{s_1} \widehat{G}^\alpha), \end{aligned}$$

and the loss term  $L_\Sigma^*$  is derived from the jump in the derivative with respect to the  $x$ -variable at the interface  $x = \alpha$ , as stated in (3.20). The corresponding training task

is given by

$$\begin{aligned} \theta^* = & \arg \min_{\theta} L_{\Omega}(\widehat{G}^{\alpha}) + \beta_{\partial\Omega} L_{\partial\Omega}(\widehat{G}^{\alpha}) + \beta_{\Gamma} \left( L_{\Gamma_1}(\widehat{G}^{\alpha}) + L_{\Gamma_2}(\widehat{G}^{\alpha}) \right) + \beta_{\alpha} L_{\alpha}(\widehat{G}^{\alpha}) \\ & + \beta_{\Sigma} \left( L_{\Sigma}(\widehat{G}^{\alpha}) + L_{\Sigma}^*(\widehat{G}^{\alpha}) \right) + \beta_{\text{sym}} L_{\Omega}^{\text{sym}}(\widehat{G}^{\alpha}), \end{aligned}$$

where  $\beta_{\Gamma}$ ,  $\beta_{\alpha}$  and  $\beta_{\Sigma} > 0$  are also user-defined penalty coefficients. Here the loss term  $L_{\Omega}^{\text{sym}}(\widehat{G}^{\alpha})$ , defined in a similar way as in (3.2), is included to improve performance. After obtaining the trained model of  $\widehat{G}^{\alpha}(\cdot; \theta)$ , the restriction  $\check{G}^{\alpha}(x, y)$  is performed the same as in (3.6).

**Appendix C. Details of the neural network training for solving the benchmark problem (2.3).** We consider the one-dimensional benchmark problem (2.3), where the Green's function takes on the form

$$(C.1) \quad G(x, y) = \begin{cases} -\frac{\sin(kx)\sin(k(y-1))}{k\sin(k)} & \text{if } 0 \leq x \leq y, \\ -\frac{\sin(k(x-1))\sin(ky)}{k\sin(k)} & \text{if } y \leq x \leq 1. \end{cases}$$

A fully-connected neural network [15] using the Tanh activation function with 4 hidden layers, each containing 40 neurons, is employed for the approximation. We randomly select 160  $x$  points in  $\Omega$  ( $N_{\Omega} = 160$ ) and for each selected  $x$  point, a corresponding set of 160  $y$  points in  $\Omega$  and 2  $y$  points on  $\partial\Omega$  ( $N'_{\Omega} = 160, N_{\partial\Omega} = 2$ ). Additionally, 500 points are sampled at the interface  $x = y$  ( $N_{\Gamma} = 500$ ). After 30,000 epochs of network training, with the parameters set to  $\beta_{\partial\Omega} = \beta_{\text{sym}} = 400$  and  $\beta_{\Gamma} = 1000$ , the final computational results are shown in Figure 1.

Given the forcing term

$$(C.2) \quad f(x) = 20 - 60\pi x \cos(20\pi x^3) + 1800\pi^2 x^4 \sin(20\pi x^3),$$

the exact solution of (2.1) is

$$u(x) = 10x - 10x^2 + 0.5 \sin(20\pi x^3),$$

which contains variation on many different frequencies [28]. The numerical solution using our neural Green's function and the approximation error are depicted in Figure 2.

### Appendix D. Proof of Theorem 3.3.

*Proof.* The training dynamics of  $\theta$  follows the gradient flow

$$(D.1) \quad \frac{d\theta}{dt} = -\nabla_{\theta} L(\theta), \quad \frac{dL(\theta)}{dt} = -|\nabla_{\theta} L(\theta)|^2.$$

Recalling (3.13), the high-frequency components flow  $L_{\eta^+}(\theta)$  is given by

$$(D.2) \quad \frac{dL_{\eta^+}(\theta)}{dt} = \left( \sum_{j=\eta}^{+\infty} \nabla_{\theta}(\gamma_j^2(\theta)) \right) \cdot \frac{d\theta}{dt} = -2 \sum_{j=\eta}^{+\infty} \gamma_j(\theta) (\nabla_{\theta} \gamma_j(\theta) \cdot \nabla_{\theta} L(\theta)).$$

Thus, using (D.2), the ratio of high-frequency decrement rate to the overall decrement rate of the loss function can be bounded by

$$(D.3) \quad \left| \frac{dL_{\eta^+}(\theta)}{dt} \right| \leq \eta^{-(1-\delta)} \frac{\sum_{j=\eta}^{\infty} j^{1-\delta} |\gamma_j(\theta)| |\nabla_{\theta} \gamma_j(\theta)|}{|\nabla_{\theta} L(\theta)|} \left| \frac{dL(\theta)}{dt} \right|.$$

Cauchy-Schwarz inequalities lead to

$$(D.4) \quad \left( \sum_{j=\eta}^{\infty} j^{1-\delta} |\gamma_j(\theta)| |\nabla_{\theta} \gamma_j(\theta)| \right)^2 \leq \left( \sum_{j=\eta}^{\infty} j^{3-\delta} |\gamma_j(\theta)|^2 \right) \left( \sum_{j=\eta}^{\infty} j^{-1-\delta} |\nabla_{\theta} \gamma_j(\theta)|^2 \right).$$

We are to estimate the two terms in (D.4) separately. Recalling the definition of  $\gamma_j(\theta)$  (3.12) and eigenfunctions  $\phi_j$  (3.2), we have

$$(D.5) \quad \begin{aligned} \sum_{j=\eta}^{\infty} j^{3-\delta} |\gamma_j(\theta)|^2 &= \sum_{j=\eta}^{\infty} j^{3-\delta} \left| \int_0^1 \int_0^1 \left( \widehat{G}(x, y, |y-x|; \theta) - G(x, y) \right) \phi_j(x) \phi_j(y) dy dx \right|^2 \\ &= \sum_{j=\eta}^{\infty} j^{3-\delta} \left| \int_0^1 \int_0^1 \widehat{G}(x, y, |y-x|; \theta) \phi_j(x) \phi_j(y) dy dx - \mu_j \right|^2. \end{aligned}$$

Actually, when  $\eta \geq \frac{k}{\sqrt{\pi^2 - 1}}$ , for every  $j \geq \eta$ , we have  $\frac{j^{3-\delta}}{(j^2 \pi^2 - k^2)^2} \leq \frac{1}{j^{1+\delta}}$ . Then with  $\mu_j$  given in (3.9), we can obtain that

$$(D.6) \quad \sum_{j=\eta}^{\infty} j^{3-\delta} (\mu_j)^2 = \sum_{j=\eta}^{\infty} \frac{j^{3-\delta}}{(j^2 \pi^2 - k^2)^2} \leq \sum_{j=\eta}^{\infty} \frac{1}{j^{1+\delta}} < \infty.$$

Next we need to prove the convergence of  $\sum_{j=\eta}^{+\infty} j^{3-\delta} \left| \int_0^1 \int_0^1 \widehat{G}(\cdot; \theta) \phi_j(x) \phi_j(y) dy dx \right|^2$ .

Before proceeding, for brevity we define

$$(D.7) \quad \widehat{\Delta}_y \widehat{G} := \partial_{yy} \widehat{G} + 2\partial_{yr} \widehat{G} \partial_y r + \partial_{rr} \widehat{G} (\partial_y r)^2.$$

We can reformulate this series with integration by parts as follows

$$(D.8) \quad \begin{aligned} &\sum_{j=\eta}^{+\infty} j^{3-\delta} \left| \int_0^1 \int_0^1 \widehat{G}(x, y, |y-x|; \theta) \phi_j(x) \phi_j(y) dy dx \right|^2 \\ &= 4 \sum_{j=\eta}^{+\infty} j^{3-\delta} \left| \int_0^1 \int_0^1 \widehat{G}(x, y, |y-x|; \theta) \sin(j\pi x) \sin(j\pi y) dy dx \right|^2 \\ &= \frac{4}{\pi^2} \sum_{j=\eta}^{+\infty} j^{1-\delta} \left( \int_0^1 \sin(j\pi x) \left( \int_0^1 \widehat{G}(x, y, |y-x|; \theta) d(\cos(j\pi y)) \right) dx \right)^2. \end{aligned}$$

The inner integration of (D.8) can be further simplified with another integration by

parts,

$$\begin{aligned}
& \int_0^1 \widehat{G}(x, y, |y-x|; \theta) d(\cos(j\pi y)) \\
&= \int_0^x \widehat{G}(x, y, |y-x|; \theta) d(\cos(j\pi y)) + \int_x^1 \widehat{G}(x, y, |y-x|; \theta) d(\cos(j\pi y)) \\
\text{(D.9)} \quad &= \widehat{G}(\cdot; \theta) \cos(j\pi y) \Big|_{y=0}^{y=x^-} - \int_0^x (\partial_y \widehat{G}(\cdot; \theta) + \partial_r \widehat{G}(\cdot; \theta) \partial_y r) \cos(j\pi y) dy \\
&\quad + \widehat{G}(\cdot; \theta) \cos(j\pi y) \Big|_{y=x^+}^{y=1} - \int_x^1 (\partial_y \widehat{G}(\cdot; \theta) + \partial_r \widehat{G}(\cdot; \theta) \partial_y r) \cos(j\pi y) dy.
\end{aligned}$$

The continuity of  $\widehat{G}$  implies  $[\widehat{G}(\cdot; \theta)]_{y=x} = 0$  and the assumption 2 derives  $\widehat{G} = 0$  on  $\partial\Omega$ , then the boundary terms

$$\text{(D.10)} \quad \widehat{G}(\cdot; \theta) \cos(j\pi y) \Big|_{y=0}^{y=x^-} + \widehat{G}(\cdot; \theta) \cos(j\pi y) \Big|_{y=x^+}^{y=1} = 0$$

vanish during the calculation. Substitute (D.7) and use (D.10), (D.9) further comes to

$$\begin{aligned}
& \int_0^1 \widehat{G}(x, y, |y-x|; \theta) d(\cos(j\pi y)) \\
\text{(D.11)} \quad &= - \left( \int_0^x (\partial_y \widehat{G} + \partial_r \widehat{G} \partial_y r) \cos(j\pi y) dy + \int_x^1 (\partial_y \widehat{G} + \partial_r \widehat{G} \partial_y r) \cos(j\pi y) dy \right) \\
&= - \frac{1}{j\pi} \left( (\partial_y \widehat{G} + \partial_r \widehat{G} \partial_y r) \sin(j\pi y) \Big|_{y=0}^{y=x^-} + (\partial_y \widehat{G} + \partial_r \widehat{G} \partial_y r) \sin(j\pi y) \Big|_{y=x^+}^{y=1} \right. \\
&\quad \left. - \int_0^x \widehat{\Delta}_y \widehat{G} \sin(j\pi y) dy - \int_x^1 \widehat{\Delta}_y \widehat{G} \sin(j\pi y) dy \right).
\end{aligned}$$

Notice that

$$\begin{aligned}
\text{(D.12)} \quad & (\partial_y \widehat{G} + \partial_r \widehat{G} \partial_y r) \sin(j\pi y) \Big|_{y=0}^{y=x^-} + (\partial_y \widehat{G} + \partial_r \widehat{G} \partial_y r) \sin(j\pi y) \Big|_{y=x^+}^{y=1} \\
&= (\partial_y \widehat{G} + \partial_r \widehat{G} \partial_y r) \sin(j\pi y) \Big|_{y=x^-}^{y=x^+} = \partial_r \widehat{G} \partial_y r \sin(j\pi y) \Big|_{y=x^-}^{y=x^+} = 2\partial_r \widehat{G} \sin(j\pi x),
\end{aligned}$$

where  $\partial_y \widehat{G}, \partial_r \widehat{G}$  is still continuous at  $y = x$ , and  $[\partial_y r]_{y=x} = 2$  according to the definition of  $r(x, y)$ .

Combining (D.9)-(D.12), (D.8) comes to

$$\begin{aligned}
& \frac{4}{\pi^2} \sum_{j=\eta}^{+\infty} j^{1-\delta} \left( \int_0^1 \sin(j\pi x) \left( \int_0^1 \widehat{G}(x, y, |y-x|; \theta) d(\cos(j\pi y)) \right) dx \right)^2 \\
\text{(D.13)} \quad &= \frac{4}{\pi^2} \sum_{j=\eta}^{+\infty} \frac{1}{j^{1+\delta}} \left( \int_0^1 \int_0^x \widehat{\Delta}_y \widehat{G} \sin(j\pi y) \sin(j\pi x) dy dx \right. \\
&\quad \left. + \int_0^1 \int_x^1 \widehat{\Delta}_y \widehat{G} \sin(j\pi y) \sin(j\pi x) dy dx - \int_0^1 2\partial_r \widehat{G} \sin^2(j\pi x) dx \right)^2
\end{aligned}$$

Notice that the derivatives of  $\widehat{G}$  including  $\partial_r \widehat{G}, \partial_{yy} \widehat{G}, \partial_{yr} \widehat{G}, \partial_{rr} \widehat{G}$  are continuous, and

the derivative of levelset function  $\partial_y r(x, y) \in C((0, x) \cup (x, 1))$ , thus

$$\begin{aligned}
& \frac{4}{\pi^2} \sum_{j=\eta}^{+\infty} \frac{1}{j^{1+\delta}} \left( \int_0^1 \int_0^x \widehat{\Delta}_y \widehat{G} \sin(j\pi y) \sin(j\pi x) dy dx \right)^2 \\
(D.14) \quad & \leq \frac{4}{\pi^2} \sum_{j=\eta}^{+\infty} \frac{1}{j^{1+\delta}} \int_0^1 \int_0^x |\widehat{\Delta}_y \widehat{G}|^2 dy dx \int_0^1 \int_0^x \sin^2(j\pi y) \sin^2(j\pi x) dy dx \\
& = \frac{1}{\pi^2} \sum_{j=\eta}^{+\infty} \frac{1}{j^{1+\delta}} \left( \int_0^1 \int_0^x |\widehat{\Delta}_y \widehat{G}|^2 dy dx \right) < +\infty.
\end{aligned}$$

Similarly, we can obtain that

$$(D.15) \quad \sum_{j=\eta}^{+\infty} \frac{1}{j^{1+\delta}} \left( \int_0^1 \int_x^1 \left( \partial_{yy} \widehat{G} + 2\partial_{yr} \widehat{G} \partial_y r + \partial_{rr} \widehat{G} \right) \sin(j\pi y) \sin(j\pi x) dy dx \right)^2 < +\infty.$$

Moreover, by Cauchy-Schwarz inequality,

$$\begin{aligned}
& \frac{4}{\pi^2} \sum_{j=\eta}^{+\infty} \frac{1}{j^{1+\delta}} \left( \int_0^1 2\partial_r \widehat{G} \sin^2(j\pi x) dx \right)^2 \\
(D.16) \quad & \leq \frac{4}{\pi^2} \sum_{j=\eta}^{+\infty} \frac{1}{j^{1+\delta}} \left( \int_0^1 4|\partial_r \widehat{G}|^2 dx \right) \left( \int_0^1 \sin^4(j\pi x) dx \right) < +\infty
\end{aligned}$$

From (D.16), (D.14), (D.15) and triangle inequality, we achieve that series (D.8) is convergent, *i.e.*

$$(D.17) \quad \sum_{j=\eta}^{+\infty} j^{3-\delta} \left| \int_0^1 \int_0^1 \widehat{G}(\cdot; \theta) \phi_j(x) \phi_j(y) dy dx \right|^2 < +\infty.$$

Next, by combining equations (D.5), (D.6) and (D.17), we conclude that the first term on the right side of (D.4)

$$(D.18) \quad \sum_{j=\eta}^{+\infty} j^{3-\delta} |\gamma_j(\theta)|^2 < +\infty$$

is convergent.

The second term on the right side of (D.4) can be bounded by Cauchy-Schwarz inequality and the smoothness of  $\nabla \widehat{G}(\cdot; \theta)$ ,

$$\begin{aligned}
& \sum_{j=\eta}^{+\infty} j^{-1-\delta} |\nabla_\theta \gamma_j(\theta)|^2 \\
(D.19) \quad & = \sum_{j=\eta}^{+\infty} \frac{4}{j^{1+\delta}} \left| \int_0^1 \int_0^1 \nabla_\theta \widehat{G}(\cdot; \theta) \sin(j\pi y) \sin(j\pi x) dy dx \right|^2 \\
& \leq \sum_{j=\eta}^{+\infty} \frac{4}{j^{1+\delta}} \int_0^1 \int_0^1 |\nabla_\theta \widehat{G}(\cdot; \theta)|^2 dy dx \int_0^1 \int_0^1 \sin^2(j\pi y) \sin^2(j\pi x) dy dx < +\infty.
\end{aligned}$$

Therefore, based on assumption 1 which guarantees a positive lower bound of denominator of (D.3) and equations (D.18) and (D.19), we obtain that there exists a constant  $C > 0$  dependent on  $\theta$  such that

$$(D.20) \quad \frac{\sum_{j=\eta}^{+\infty} j^{1-\delta} |\gamma_j(\theta)| |\nabla_{\theta} \gamma_j(\theta)|}{|\nabla_{\theta} L(\theta)|} \leq C,$$

which indicates (3.14).  $\square$

**Appendix E. Details of solving the eigenproblem (3.9).** It is easy to check the orthogonality and completeness

$$\sum_{j=1}^{\infty} \phi_j(x) \phi_j(y) = \delta(x-y) \quad \text{and} \quad \int_0^1 \phi_m(x) \phi_n(x) = \delta_{mn} \quad \text{for } m, n > 0.$$

Here, we employ the quadratic elements with meshwidth  $h = 2^{-10}$  on a uniform mesh grid, with the relative errors defined as

$$\epsilon_{\mu} = \frac{|\mu_j - \hat{\mu}_j|}{|\mu_j|} \quad \text{and} \quad \epsilon_{\phi} = \frac{\|\phi_j(x) - \hat{\phi}_j(x)\|_{L^2(\Omega)}}{\|\phi_j(x)\|_{L^2(\Omega)}},$$

shown in Figure 10.

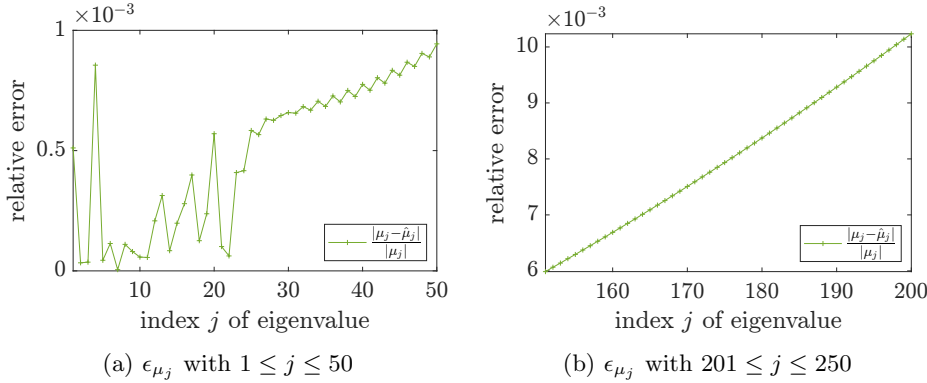


Fig. 10: Relative errors of eigenpairs computed with neural Green's function for model problem (2.3).